MATERIALS CHEMISTRY
FRONTIERS

REVIEW

View Article Online
View Journal | View Issue

Cite this: *Mater. Chem. Front.*, 2024, **8**, 3528

Interface passivation strategies for high-performance perovskite solar cells using two-dimensional perovskites

He Huang,† Xiaobo Zhang,† Wencai Zhou, Yong Huang, Zilong Zheng,* Xiaoqing Chen,* Yongzhe Zhang* and Hui Yan

Received 2nd July 2024,
Accepted 9th September 2024

DOI: 10.1039/d4qm00560k

rsc.li/frontiers-materials

The performance of perovskite solar cells (PSCs) is critically influenced by the quality of interfaces, including grain boundaries and perovskite surfaces. These interfaces are often highly defective, leading to non-radiative recombination and impaired charge transfer. Additionally, operational conditions can induce undesirable chemical reactions, affecting long-term stability. This review summarizes advancements over the past five years in achieving high-efficiency (near or above 25%) through interface passivation. Notably, using two-dimensional/three-dimensional (2D/3D) hybrid perovskites, which combine the stability of 2D perovskites with the efficiency of 3D perovskites, has emerged as a promising strategy. We reviewed recent progress in interface passivation strategies, focusing on the implementation of 2D/3D perovskite passivation across buried interfaces, grain boundaries and top interfaces. Finally, we discussed challenges and future directions for multi-interface cooperative passivation, charge dynamics and degradation mechanisms.

1. Introduction

Metal halide perovskites have garnered significant attention as a revolutionary class of semiconductor materials, primarily due to their exceptional physical and chemical properties. These materials exhibited ultra-high optical absorption coefficients (exceeding 10^5 cm^{-1}), tunable bandgaps (ranging from 1.4 eV to 2.5 eV), long carrier diffusion lengths (more than 1 μm), and high defect-tolerance.[1–6] These qualities make these perovskites widely applicable in various domains such as solar cells, photodetectors, and lasers.[7,8] In the field of photovoltaics, perovskite solar cells (PSCs) have exhibited power conversion efficiency (PCE) reaching 26.54%,[9] which is comparable to around 26.81% of commercial crystalline silicon cells.[10] Despite these impressive efficiencies, the instability of perovskite materials under conditions such as temperature fluctuations, oxygen, humidity and light exposure remains a significant barrier to their commercialization.

To address the instability issues, researchers have identified two-dimensional (2D) perovskites as more thermally, chemically and environmentally stable compared to their three-dimensional (3D) counterparts.[11–13] However, pure 2D PSCs (19.24%[14]) typically exhibit lower PCE than 3D PSCs. This performance gap is mainly attributed to a wider optical band gap (>2 eV) of 2D perovskites, which results in partial light absorption loss, and their lower carrier diffusion coefficients, which hinder effective charge transport across organic cation interlayers.[15–20] Therefore, leveraging the high stability of 2D perovskites, while maintaining the high efficiency characteristics of 3D perovskites is a challenge. This has led to increasing interest in mixed-dimensional 2D/3D perovskite structures, which aim to combine the advantages of both dimensions while mitigating their respective weaknesses.

Emerging 2D/3D hybrid perovskite structures have shown promise, with achieved efficiency being as high as 25.6%.[21] These structures are usually constructed by introducing long chain organic spacer cations, which are not suitable for 3D perovskite frameworks, into the interfaces of the bulk perovskite materials. The variations in molecular structures, functional groups, organic cation concentrations, and other synthesis conditions lead to diverse 2D/3D structures with different performances.[22] Despite this diversity, the PCE improvement mechanism of 2D/3D hybrid structures is generally attributed to effective interface passivation.[23]

This review aims to summarize recent advancements in achieving high efficiency PSCs (near or above 25%) through interface passivation strategies over the past five years. We observed that the most high-efficiency PSC research studies focused on interface passivation, and frequently employed 2D/

College of Materials Science and Engineering, Faculty of Information Technology, Beijing University of Technology, Beijing, 100124, P. R. China.
E-mail: zilong.zheng@bjut.edu.cn, chenxiaoqing@bjut.edu.cn, yzzhang@bjut.edu.cn
† He Huang and Xiaobo Zhang contributed equally to this paper.

3D perovskite methods. Therefore, we begin by discussing the most commonly reported organic ammonium salt precursors and then explore rational design strategies for other precursors and methods for low-dimensional perovskite crystallization. Following this, we delve into methodologies for implementing these strategies at three critical interfaces: buried interfaces, grain boundaries and top interfaces. Finally, we discussed current challenges and future directions in the realm of 2D perovskite passivation agents, including multi-interface cooperative passivation, charge dynamics and degradation mechanisms. The optimization of interface passivation strategies, especially those involving 2D/3D hybrid perovskite structures, holds significant potential for enhancing the efficiency and stability of PSCs, paving the way for their commercial viability.

2. Strategies of 2D/3D perovskite passivation

Passivation refers to treatment that renders a material less sensitive, less reactive, or more corrosion-resistant.[24] Since the 1980s, surface passivation has been employed in crystalline silicon solar cells to achieve PCE exceeding 20%.[25] Recently, interface passivation becomes critical for the rapid development of PSCs, significantly boosting their efficiency and stability.[21,26–33]

The 2D/3D passivation strategy for PSCs was first introduced by Li *et al.* in 2017.[34] They introduced PEA^+ cations into the $FAPbI_3$ perovskite, revealing that PEA^+ can assemble at interfaces to form 2D/3D perovskite structures, thereby passivating surface defects and improving both phase and moisture stability. In 2020, Sutanto *et al.* demonstrated that a 2D perovskite capping layer protected the underlying 3D bulk perovskite from degrading into lead iodide, further enhancing its stability.[35] Furthermore, the 2D/3D structure improved crystallinity and reduced defects responsible for non-radiative recombination, leading to a reduction in the voltage–current hysteresis.[11] Consequently, the 2D/3D perovskite passivation strategy significantly improves the efficiency and stability of PSCs. It is worth noting that many studies do not explicitly distinguish the roles of 2D perovskites as capping layers *versus* molecular passivation layers. The passivation layer may also form a 2D perovskite layer, and the 2D perovskite layer itself may serve as a passivation layer.

The mechanisms through which 2D perovskites passivate interfaces include:[15–20] (1) passivation of surface defects such as dangling bonds, interstitial defects and vacancy defects at the interface, (2) optimization of the energy level alignment to promote carrier transport across the interface between the perovskite and charge transport layers, (3) enhancement of moisture resistivity *via* hydrophobic long chain groups in the 2D perovskite, (4) improvement of thermal stability due to the strong interaction between 2D organic cations and iodide, and (5) inhibition of ion migration through restriction imposed by the anisotropy of 2D perovskites.

In this review, we focus on the role of passivation played by 2D perovskite layers discussing on outstanding works reported related to ultra-high efficiency PSCs. We summarized the 2D/3D interface passivation strategies, classifying them according to various pathways: formation of passivators, rational design, and specific crystallization methods to achieve interface passivation.

2.1 Organic ammonium salts as 2D perovskite precursors

The interface of a 2D perovskite is usually formed *in situ* through a reaction between residual excess PbI_2 at the interface and organic halide salts, such as butylammonium iodide (BAI), phenylethyl ammonium iodide (PEAI), and octyl ammonium iodide (OAI).[36–38] Different organic halide salts could form distinct 2D perovskite structures with varied performances. Among these, PEAI, composed of PEA^+ cations and I^- anions, is the most frequently employed precursor in the interface passivation of high-efficiency PSCs.[39–49] Given its prevalence, we will begin our discussion on 2D/3D perovskite passivation strategies with PEAI and its derivatives, before exploring other precursors containing different types of long-chain organic cations.

2.1.1. PEAI and its derivatives. In 2016, Wang *et al.* for the first time reported the application of a PEAI (a salt composed of PEA^+ and I^-) passivation perovskite interface to improve the performance, in which a small sized hydrophobic aromatic group and the edge-on packing of the benzene rings on the perovskite surface were formed.[50] Surprisingly, the organic halide salt PEAI, rather than the 2D layered PEA_2PbI_4 perovskite proposed in other studies,[51] serves as a much more effective passivation additive for a 3D perovskite. And similar articles have been reported by Wang and Jiang. Wang *et al.* found that it was difficult to form a 2D or quasi-2D perovskite capping layer by post-treatment of the $CsPbI_3$ surface using PEAI through either solid state or sequential cation exchange instead of using a defect-passivating organic cation terminated surface.[52] Jiang *et al.* carefully controlled the conversion process of PEAI to PEA_2PbI_4 in the actual devices using direct XRD evidence and showed the existence of PEAI instead of PEA_2PbI_4 in the perovskite thin-film devices, which played the key role in increasing the PCE to as high as 23.32%, which was the highest in 2019 (Fig. 1a).[47]

The PCE improvement by PEAI is mainly attributed to the suppression of the undesirable surface properties that impede carrier transport and induce recombination. Wang *et al.* used ultrafast transient transmission and reflection microscopy to distinguish the near-surface and bulk carrier diffusion coefficients, which found that PEAI surface functionalization increased the diffusion coefficient of the carriers in the 40 nm subsurface region from 0.6 to 1.0 $cm^2\ s^{-1}$ similar to the value for bulk carriers resulting from both reduced electron–phonon scattering and defects on the perovskite surface (Fig. 1b).[53]

Aside from the improved PCE, PEAI was found to form a 2D perovskite to improve the stability of PSCs. For example, Zhu *et al.* successfully introduced two-dimensional nanoplates between perovskite grain boundaries by introducing PEAI, which remarkably improves the humidity and thermal stability (retained 85% and 90% of its initial PCE value after storing for 200 h in ~85% humidity and for 500 h at 100 °C, respectively, Fig. 1c).[51]

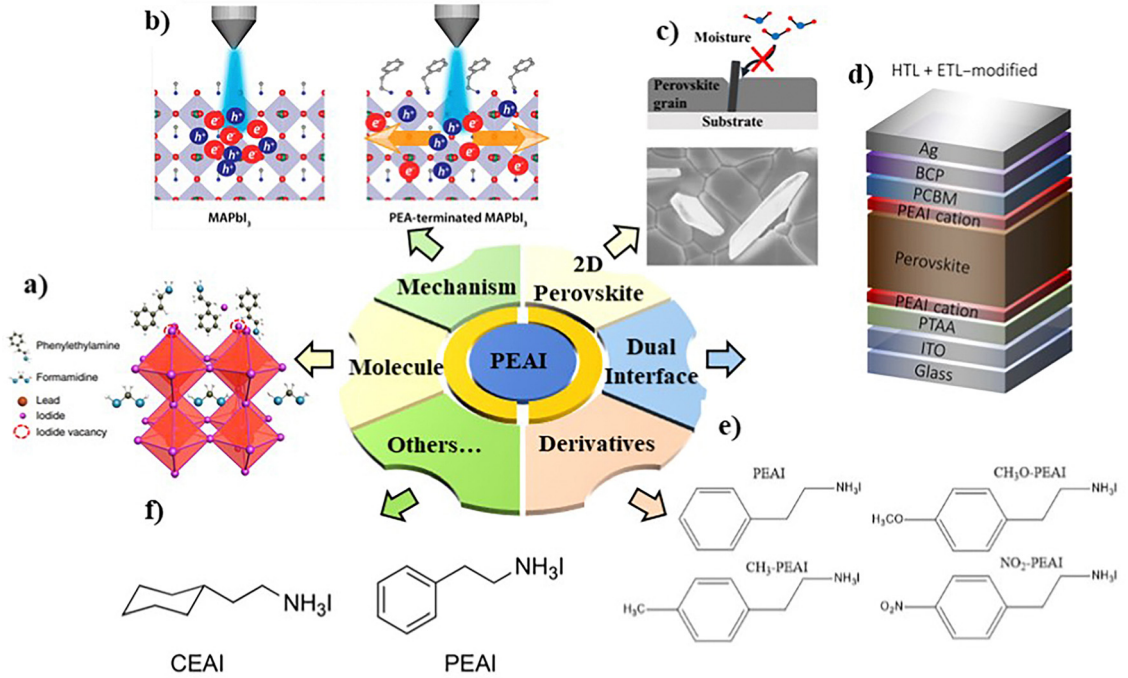

Fig. 1 (a) PEAI passivation of a perovskite surface.[47] (b) Schematic diagram of carrier diffusion on the perovskite and PEA-terminated perovskite surface.[53] (c) Modification of grain boundaries by PEA_2PbI_4 nanoplates.[51] (d) Dual interface (HTL/perovskite and ETL/perovskite) passivation using PEA-based organic cations.[54] (e) PEAI derivatives with different functional groups.[55] (f) Structure comparison between CEAI and PEAI.[56]

Feng *et al.*[57] also found that Eu–porphyrin complexes (Eu–pyP) acted as 2D $(Eu\text{–}pyP)_{0.5}MA_{n-1}Pb_nI_{3n+1}$ platelets inlaying the GBs of 3D polycrystalline interstices to improve perovskite stability.[37,41,47,55,58–61]

Further than single-surface passivation, PEAI and its derivatives can realize double-surface modification. Recently, Grancini's group presented a dual interfacial modification approach by inserting PEA-based organic cations at both the bottom and top perovskite interfaces (Fig. 1d). The modification of the bottom interface led to an improved wettability, which eliminates the formation of nano-voids at the interface with the HTL. And the modification of the top perovskite surface led to its efficient passivation and a reduction in nonradiative recombination losses. Next, the dual interface modification approach was effectively combined with the incorporation of ionic liquids into the perovskite active layer, leading to both efficient and stable improvement, reaching a maximum PCE of 23.7%.[54] More interestingly, Mahmud *et al.* modified the uniform double-sided passivation strategy by using a discontinuous 2D perovskite (BAI) layer, which passivated the interface without sacrificing the charge transport,[62] similar to that of TOPC on silicon solar cells.

PEAI has been modified to various derivatives by adding functional groups to PEA^+ (Fig. 1e),[55] which further improved the passivation effect compared to that of PEAI in the 2D perovskite interface passivation. For example, Li *et al.* introduced a novel brominated passivator 2-bromophenethylammonium iodide (2-Br-PEAI) with multiple passivation functions at a perovskite interface. It not only formed a 2D perovskite on top of the 3D perovskite but also created multi-interactions (halide vacancy filling, anion bonding ability and interaction of hydrogen bonding N–H···Br with FA cations and $[PbI_6]^{4-}$) with the 3D perovskite surface.[63] In addition to using PEAI and its derivatives, there are some passivators similar to PEAI but with different main structures, which are constructed to form 2D/3D structure passivation interfaces.

2.1.2. Other types of 2D long-chain organic cations. To further improve the efficiency and stability of PSCs, more and more organic long-chain cations are being developed to replace the PEA^+ (and derivative) ions, such as BA^+, OA^+ *etc.* Xu *et al.* illustrated that 4-(aminoethyl)pyridine (4-AEP), a kind of long-chain cation, would induce a 2D crystal phase with a lower *n*-value at the 3D grain boundaries, while PEA would induce a quasi-2D phase with a higher *n*-value. As a result, the 4-AEP incorporated $MAPbI_3$ (2D/3D) PSCs exhibited a higher power conversion efficiency (PCE, 20.7%) and exhibited better moisture resistance and long-term stability than those of the PEA based quasi-2D/3D ones (PCE, 18.8%).[64] Similarly, Yang *et al.* inspired by well-established passivation salts containing benzene rings like PEAI used cyclohexylethylammonium iodide (CEAI) with a weaker (compared with PEAI) intramolecular interaction to prevent undesirable aggregation and passivate the surface defects, leading to a more uniform film and reduced nonradiative recombination (Fig. 1f).[56]

BAI is widely used as a passivation material to construct 2D/3D passivation layer structures. In 2018, Jokar *et al.* investigated the doping effect of bulky organic cations with ethylenediammonium diiodide ($EDAI_2$) and butylammonium iodide (BAI)

as additives to passivate surface defects in tin-based perovskite solar cells. They found that the addition of BAI altered significantly the orientation of crystal growth and improved the connectivity of the crystal grains.[65] Simultaneously, BAI was applied to construct 2D/3D hybrid structures to achieve the passivation effect. For example, Zou *et al.* developed an *n*-butylammonium iodide (BAI) post-treatment process to fabricate a 2D-3D hybrid perovskite with a thin layer of 2D perovskite covered on the surface of the 3D $CH_3NH_3PbI_3$ perovskite. The chemical reaction between BAI and the residual PbI_2 improves stability and reduces the number of crystal defects of the 3D perovskite with an optimized stoichiometry, leading to a PCE of 18%.[66]

Like BAI, octylammonium iodide (OAI) is also a long-chain passivator which is frequently used to enhance the performance of PSCs. Recently, Lee *et al.* demonstrated combining *n*-octylammonium iodide (OAI) and 1,3-diaminopropane (DAP) can effectively suppress the grain boundary defects and ion migration through grain boundaries by the synergistic effect of OAI and DAP, resulting in improved efficiency and stability of PSCs. In this work, they also revealed that a mixed ammonium ligand passivation strategy (MAPS) not only enhances crystallinity and reduces grain boundaries but also improves charge transport while suppressing charge recombination. A MAPS-based opaque PSC shows the best power conversion efficiency (PCE) of 21.29% with improved open-circuit voltage (V_{OC}) and fill factor (FF), and retained 84% of its initial PCE after 1900 h at 65 °C in a N_2 atmosphere.[67] Besides, Lv *et al.*[68] introduced hexylammonium iodide (HAI) to form a HAI-derived 2D perovskite, which is reported to be more efficient in decreasing interfacial defects than the BAI-derived 2D perovskite (Fig. 2a), and achieved a PCE of 20.62% (3D + HAI) as compared to 18.83% (3D). Moreover, the long-term durability of the corresponding PSCs against humidity and heat is simultaneously improved.

However, the mechanisms of these long-chain cation passivators are still under debate. For example, Zhang *et al.* constructed a thin BAI layer on the $CH_3NH_3PbI_3$ surface, which was then transformed into either a 2D perovskite layer (BA_2PbI_4) or the organic salt itself by controlling the post-annealing process. According to the surface morphologies, the BA_2PbI_4-passivated perovskite films show lower root mean square roughness than BAI-treated films (Fig. 2b). This indicates that BA_2PbI_4-passivation is more easily achieved at the grain boundaries than BAI-passivation, which enabled achieving a PCE of 20.6% in the modified inverted perovskite solar cells in 2021.[69] Similarly, Jiang *et al.* reported that PEAI itself shows a much better passivation effect than the 2D perovskite of PEA_2PbI_4 in their work.[47] However, almost all of the passivation works default that compared to 2D layered perovskite PEA_2PbI_4,

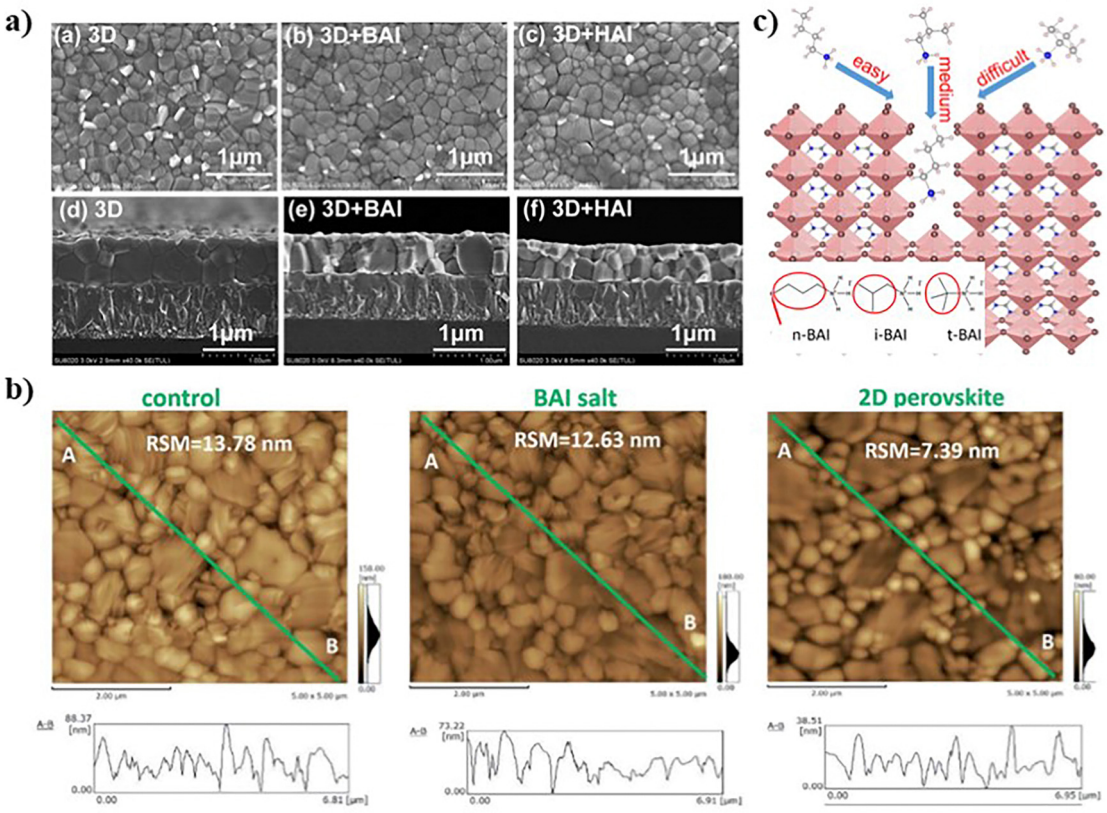

Fig. 2 (a) Top view and cross-sectional view of SEM images of different perovskite films: 3D, 3D + BAI, and 3D + HAI deposited on the top of the SnO_2 layer.[68] (b) AFM images of the control, BAI-passivated, and BA_2PbI_4-passivated perovskite films.[69] (c) Schematic diagram of BA^+ diffusion at the perovskite grain boundary.[70]

organic halide salt PEAI is a more effective passivator for 3D perovskites,[51] and the same applies to BAI and other long-chain cations.

The steric hindrance of the long-chain cations plays an important role. To reveal this effect, Zhao *et al.* explored BAI derivatives with different steric hindrances, namely, *n*-BAI, *iso*-BAI (*i*-BAI), and *tert*-BAI (*t*-BAI). They found that the efficiency and humidity stability of devices gradually increase in the order of *t*-BAI-, *i*-BAI-, *n*-BAI-modified ones (Fig. 2c), and reducing the steric hindrance (*t*-BAI-, *i*-BAI-, *n*-BAI-, in the descending order) is favorable for BAI diffusion to the grain boundary, thereby improving the grain boundary passivation effect and resulting in the formation of a residue of excessive BAI on the surface of perovskite films. A device modified with *n*-BAI shows the highest power conversion efficiency (PCE) of 20.67% with excellent stability in air with a humidity of 20–30%, retaining 80% of the original PCE after 60 days.[70]

2.2 Rational design of 2D perovskites

Building on the success of PEAI (and derivatives) and other 2D long-chain cations in interface passivation, recent optimization efforts have focused on introducing functional groups to those long-chain cations, investigating high *n*-value 2D perovskites, optimizing orientation of 2D perovskites along the *Z* axis (perpendicular to the perovskite plane) and exploring unique molecular/electronic structure designs. These advanced strategies have emerged as new focal points in the field. In this section, we review the rational design of 2D perovskite passivation cations, emphasizing how subtle differences in the molecular structure can lead to varying passivation effects.

2.2.1. Modification group attached to a long-chain cation. Strategies based on PEAI and other long chain cation defect passivation and dimensional engineering have been widely employed to improve the performance of 3D perovskites. Actually, due to the use of single passivation molecules, the strategies reported so far are difficult to simultaneously realize crystallization modulation and thorough passivation. This challenge has been overcame indirectly by introducing functional branch chains (such as Cl^-, F^-, methyl, methoxyl and so on) into organic passivation molecules.

Using halogen elements for functional group modification is a straightforward and effective method to achieve passivation. Different halides bring different passivation effects which is related to the binding energy between passivating molecules and perovskite layer materials. Liu reported that glycine-X (Gly-X, X = Cl, Br, I) can not only modulate the crystallization process of the $CsPbI_2Br$ perovskite to increase crystal quality but also generate a 2D Gly_2PbI_4 perovskite along the GBs of the 3D $CsPbI_2Br$ perovskite to block the migration of halide ions and enhance the photostability of the perovskite (Fig. 3b). As a result, the champion device based on the 2D/3D hybrid configuration exhibited an excellent stability. An unencapsulated device retained 96.6% of its initial efficiency after 50 day storage in ambient air, and the efficiency of the encapsulated device decreased only by 14.1% after 340 h continuous illumination (AM 1.5) under ambient conditions.[71]

Additionally, it is worth mentioning that this functional group modification has also proven effective in recent research with the highest PCE. Chen *et al.* fabricated a benzenesulfonate-based (BZS) new passivation molecule which could align parallel on the perovskite surface. Their research aimed to solve the problem that previously reported passivation molecules aligned in a perpendicular packing manner on a surface resulting in an uneven interface. Therefore, in their molecular design, they considered three passivation molecules with additional binding sites by introducing different functional groups, including BZS, 4CH_3-BZS and 4Cl-BZS (Fig. 3c). The results showed that conf-para (ligands adopted a parallel orientation with respect to the perovskite surface) was energetically more favorable for 4Cl-BZS because of the additional Pb^{2+} surface binding provided by the Cl functional groups (Fig. 3d and e). Based on this, they report a certified quasi-steady state PCE of 26.15% for a 0.05 cm^2 illuminated area, which is a record PCE at that time.[72]

Besides, the increased polarity by the fluorine atom can promote the growth of perovskite grains.[59] Khadka *et al.* introduced a fluoroarene anchored functional material, pentafluorophenylhydrazine (5F-PHZ), for interface treatment onto the 3D $FA_{0.84}Cs_{0.12}Rb_{0.04}PbI_3$ film. The 5F-PHz treatment improved the optoelectronic properties and provided a polar environment for the better crystallization of the perovskite, coupled with a relatively shallower defect level E_{t1}, $E_{t2} \approx 0.254$, 0.405 eV in the control device, E_{t1}, $E_{t2} \approx 0.237$, 0.378 eV in the device with 5F-PHZ with suppression of defect densities (N_{t1}, $N_{t2} \approx 1.36 \times 10^{17}$, 8.76×10^{16} cm^{-3} for the control device to N_{t1}, $N_{t2} \approx 3.28 \times 10^{16}$, 4.26×10^{16} cm^{-3} for the 5F-PHZ treated device). This approach enhanced the device performance to as high as 22.29% with superior operational stability.[73]

In order to improve the performance of PSCs further, researchers have explored different functional groups. Zhuang *et al.* investigated the passivation effect of PEAI derivatives modified with four different functional groups (Fig. 3a), finding that PEAI with electron-donating groups (methoxyl and methyl) presented more favorable passivation effects than the salt with electron withdrawing groups (nitro) that delivered undesirable impacts.[55] Thus, the addition of different functional groups causes different modifications in the interface passivation.

2.2.2. *N*-Value regulation of 2D perovskites. The *n*-values have been proven to influence optical bandgaps (E_g) of perovskite materials. Large-*n* 2D halide perovskites have low formation energies, smaller bandgaps and larger light absorption ranges, which favor the fabrication of high-efficiency PSCs.[74] Especially, the *n*-values of 2D/3D perovskites directly influence the 2D quantum-confinement effect (Fig. 4a), which provides additional modulation in the electronic structure design.[30,74] The organic–inorganic quantum well structure of 2D/3D is shown in Fig. 4a. One feasible approach for overcoming the higher bandgap value of 2D perovskites is mixing 2D/3D perovskites as the absorption layers to decrease both the optical bandgap and exciton binding energy together with enhancing the charge collection efficiency (Fig. 4b). Therefore, we reviewed several strategies for regulating the *n* values of 2D perovskites, including rational molecule design,

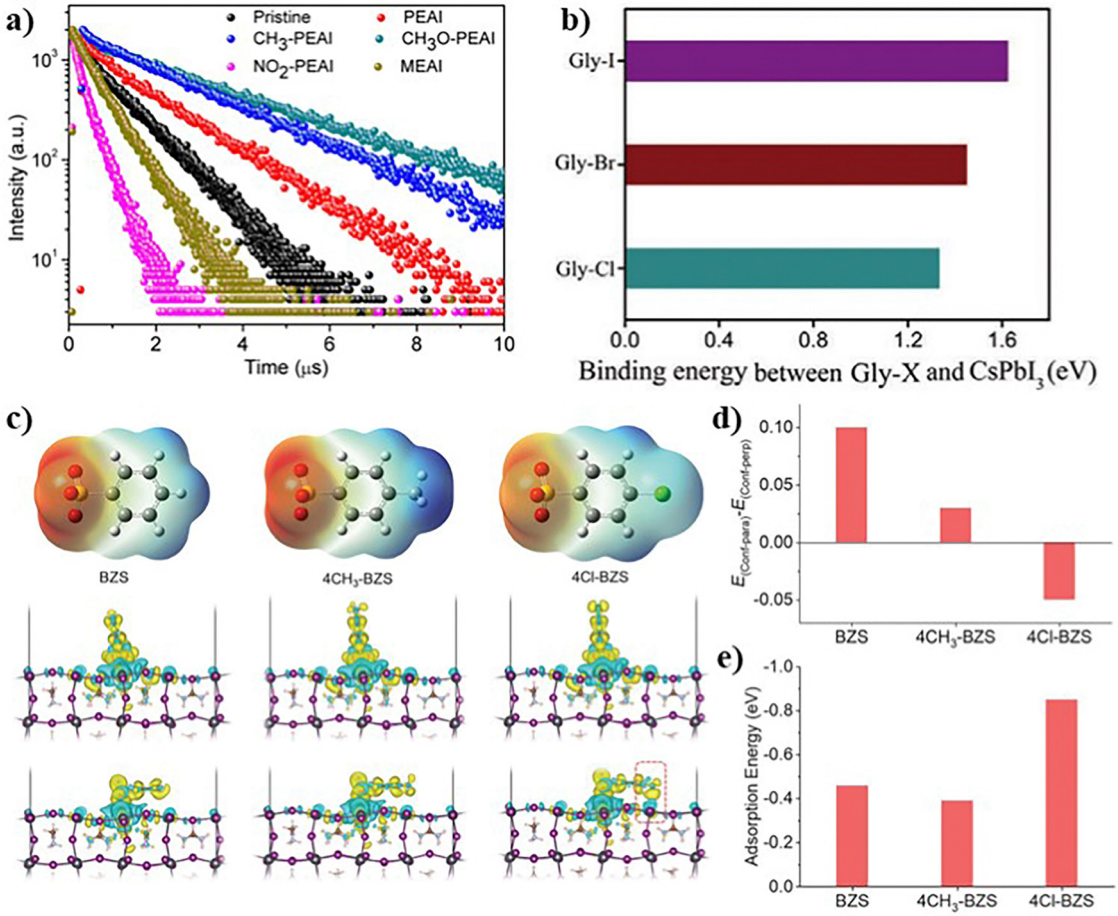

Fig. 3 (a) Time-resolved PL characterization of the passivation effect on the perovskite films by different organic ammonium iodide salts treatments.[56] (b) The calculated binding energy between Gly-X and $CsPbI_3$ by DFT.[71] (c) Structure and electrostatic potential, perpendicular orientation (Conf-perp) and planar or parallel orientation (Conf-para) on the perovskite surfaces of BZS, $4CH_3$-BZS, and 4Cl-BZS ligands. (d) Formation energy difference between parallel and perpendicular ligand-surface orientations, and (e) the adsorption energies of C60 with BZS, 4CH3-BZS, and 4Cl-BZS adsorbed on the perovskite surface.[72]

annealing temperature control and tailor-made processing solvents.

In general, perovskite films at 2D/3D interfaces without any special processing show spatially graded n values. For example, Bai *et al.* constructed a 3D–2D ($MAPbI_3$–$PEA_2Pb_2I_4$) graded perovskite interface (confirmed by the ToF-SIMS depth profile results) in which the intensity of the PEA^+ fragment decreased steeply at the near-surface of the film and then settled at a steady level much lower than that of MA^+, indicating the successful deposition of an ultrathin layer of PEA^+ on the perovskite surface. This 3D–2D graded interface provides a continuous upshift of the LUMO level, which facilitates the charge transfer from the perovskite to PCBM. At the same time, the higher LUMO level of the 3D–2D graded perovskite prevents the backflow of electrons from PCBM to the perovskite, thus suppressing the charge recombination. The consequent reduced interface charge recombination leads to an ultrahigh V_{OC} at 1.17 V.[77]

Firstly, rational molecule design can regulate the n value of 2D perovskite layers. Chen *et al.* discussed why different ligands produce different low-dimension perovskite distributions. *In situ* transient absorption spectra of a spin coated quasi-2D perovskite indicated that π–π stacking ligands form wider low-dimension perovskites (higher n) due to slower crystallization. In addition, they calculated the formation energies for each ligand (Fig. 4c), showing that only 3F-PEA shows preference for $n \geq 3$. They discovered that a large spacer cation forms a 2D heterostructure slowly, resulting in wider RDPs; and that tailor-made fluorine atom position in PEA molecules in 3F-PEA could slow down the nucleation rate of a large-n value 2D perovskite, resulting in changing or regulation of the formation energy, consequently inducing preferential growth of $n \geq 3$ low-dimension perovskites. Leveraging these insightful findings, their group developed efficient inverted PSCs (with a certified quasi-steady-state PCE of 23.91%). Unencapsulated devices operate at room temperature and around 50% relative humidity for over 1000 h without loss of PCE.[30]

Du *et al.* used *in situ* GIWAXS measurements to reveal the mechanism of the formation process of the 2D/3D perovskite structures. Their results showed that the GAI organic ligand

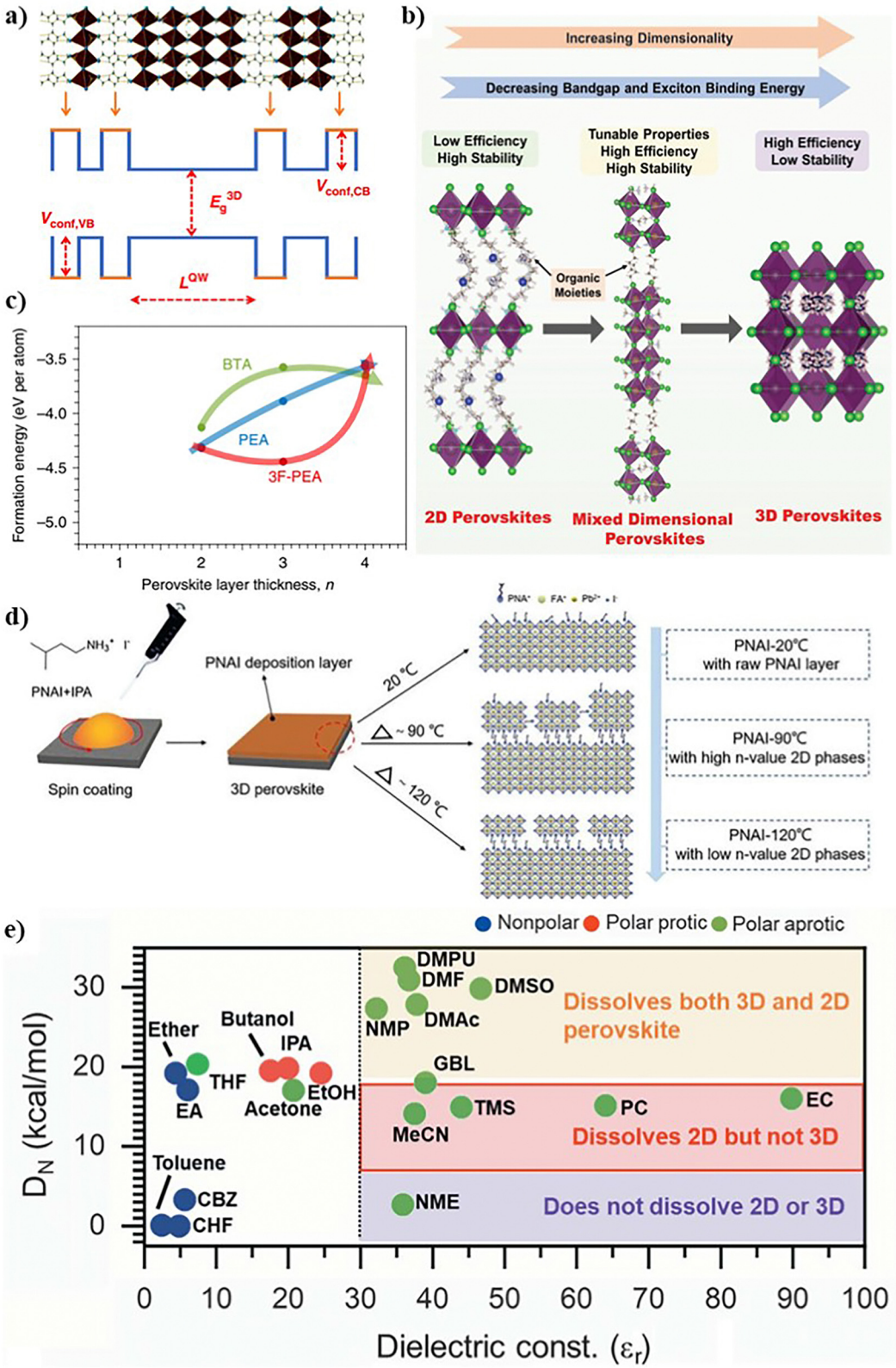

Fig. 4 (a) Schematic of a 2D/3D perovskite structure and possible energy-level schemes that can arise within these structures, where semiconducting inorganic sheets alternate with organic layers having much wider bandgaps, resulting in a Type I quantum well structure. (b) Illustration of a 2D crystalline structure, mixed-dimensional 2D/3D perovskites, and 3D perovskites. (c) The formation energy of different RDPs dependent on the layer width *n* and the ligands (BTA, PEA and 3F-PEA).[30] (d) The fabrication processes using different interfacial treatments.[75] (e) Plot showing different solvents based on the dielectric constant and the Gutmann number to identify the differences in solubility of the 3D and 2D perovskite powders for making a 3D/2D bilayer stack.[76]

formed a $n = 1$ 2D phase, and BAI formed both the $n = 2$ and the $n = 1$ 2D phases while PBAI could convert part of the 3D $CsPbI_3$ surface into a 2D perovskite with larger n values ($n = 3$) at the first stage and subsequently form a 2D perovskite with smaller n values ($n = 2$ and $n = 1$). The difference in the crystallization process is mainly attributed to the difference of the effective radii (GAI < BAI < PBAI) and reactive sites (PBAI < BAI < GAI). Moreover, only BAI could spontaneously form 2D quantum wells with a graded bandgap which was ideally aligned with the 3D perovskite, thereby facilitating the charge carrier separation and transport at the perovskite/HTL interface. The solar cells based on ambient-air blade-coated $CsPbI_3$ with a 2D/3D structure exhibited a PCE of 20.33%, which was the highest reported value for the PSCs based on printed $CsPbI_3$.[78]

Moreover, control of annealing temperature can affect the n value of 2D perovskite layers. He *et al.* introduced isopentyl ammonium iodide (PNAI) as the large organic ammonium salt to *in situ* grow high n-value 2D phases ($n \geq 3$, n is the number of inorganic layers). They found thermal treatment can affect the n-value of the 2D perovskite and the residual amount of PbI_2 (Fig. 4d). PNAI-90 treatment (annealing at 90 °C) was more likely to form high n-value 2D phases, reducing the confinement within the 2D capping layer to reduce the electron barrier between the 3D and 2D layers, leading to an effective carrier transport pathway in the 2D–3D heterojunction. Consequently, this treatment strategy significantly improves the efficiency of planar PSCs to 22.62% with an outstanding open-circuit voltage of 1.16 V. Moreover, the unencapsulated PNAI-90 treated devices retain 89% of their initial PCE after storing under a relative humidity of 30 ± 5% for 1000 h.[75]

Furthermore, tailor-made processing solvents can also affect the n value of 2D perovskite layers, namely, the ligand solution with a certain concentration can form a 2D perovskite with specific n values. Proppe *et al.*[29] showed progressive dimensional reduction from 3D to $n = 3 \rightarrow 2 \rightarrow 1$ when the $(MAPbBr_3)_{0.05}(FAPbI_3)_{0.95}$ perovskite was exposed to vinylbenzylammonium ligand cations during spin-coating, which is evidenced by *in situ* GIWAXS. DFT simulations suggested that ligands incorporate sequentially into the 3D lattice, driven by phenyl ring stacking, progressively bisecting the 3D perovskite into lower dimensional fragments to form stable interfaces. In addition, they also posited that increasing the concentration of IPA in the ligand solution facilitated the interface formation, resulting in thicker and more disordered RDP layers, thus leading to poorer charge extraction at 2D/3D interfaces.

Sidhik *et al.* found that processing solvents with dielectric constant $\varepsilon_r > 30$ and Gutmann number, $5 < DN < 18$ kcal mol^{-1} could effectively dissolve the 2D perovskite powders without dissolving or degrading the underlying 3D perovskite film during processing by using spin coating. This is because the dielectric constant (ε_r) and the Gutmann donor number (DN) can regulate the coordination between the precursor ions and the solvent (Fig. 4e). They also used different n values and film thicknesses to progressively tune the heterostructure from type I to type II, thus successfully promoting the charge extraction at the 2D/3D interface. Based on the stacking of a phase-pure two-dimensional (2D) halide perovskite with the desirable composition, thickness, and bandgap onto 3D perovskites without dissolving the underlying substrate, they achieved a 5PCE of 24.5%, with exceptional stability of T_{99} (time required to preserve 99% of initial photovoltaic efficiency) of >2000 hours.[76]

2.2.3. Orientation optimization. A slight difference of a 2D perovskite molecular structure will have a strong impact on the preferred orientation of crystallization. DJ type 2D perovskites (such as 2,2′-ethylenedioxy-bis-ethylamine, EDOEA) were used as the optimal crystallinity regulator for perovskite nucleation and crystal growth with a preferential orientation and for availably releasing tensile stress.[79] Regarding this, Zhong *et al.* also confirmed that reoriented perovskite crystals were related to the binding energy and the hydrogen-bonding interaction between $[PbX_6]^{4-}$ layers and diammonium spacer cations with different molecular configurations (octane-1,8-diamine, ODA, triethylenetetramine, TETA, and EDOEA, Fig. 5a). And another type of 2D perovskite, an RP molecular structure, is also used to control the preferred orientation of crystallization. Choi *et al.* used a vacuum deposition method to obtain a highly ordered butylammonium-RP perovskite layer in the out-of-plane direction, which enables solving the charge transport problem because of the traditional RP perovskite's anisotropic structural features (Fig. 5b and c). Benefitting from this passivation and hydrophobic layer, the PCE of a BABr-based inverted PSC was enhanced to 21.4% with high humidity/thermal stability.[80]

Besides, Jeong *et al.* used a simple post-treatment to introduce the novel 2D layered perovskites with a preferred orientation in the direction of [002] for CHA_2PbI_4 (CHAI = cyclohexyl ammonium iodide) and $CHMA_2PbI_4$ (CHMAI = cyclohexyl methylammonium iodide), which promotes the charge transport. Theoretical simulations demonstrated that the graded n-value perovskite phase can spontaneously form due to the low formation energy of CHA_2PbI_4 (−2.71 eV) and $CHMA_2PbI_4$ (−3.03 eV), and funnel-like energy level alignment during surface treatment, resulting in efficient charge transport. Notably, both 2D perovskite films feature the preferred oriented planes of (002). As a result, the devices with a 2D/3D perovskite heterojunction exhibited an improved PCE from 20.41% to 23.91% primarily because of the increased open-circuit voltages (1.079 to 1.143 V) and fill factors (78.22% to 84.25%).[82]

Changing the seeds of perovskite crystallization can also realize its orientation adjustment and optimization. Luo *et al.* proposed a seed-induced growth method, in which highly oriented 2D $(BDA)PbI_4$ perovskites were used as seeds to optimize the growth kinetics of 3D perovskite and confine its crystallization directly to stride over the nucleation stage (Fig. 5d). In the crystallization process, the 2D perovskite seeds firstly acted as templates to epitaxially grow a 3D perovskite with the desired facet orientation and stacking mode. And then, these seeds would transform into the grain boundary to improve the stability. As a result, the high-quality mixed-dimensional perovskite film delivers a superior PCE of 23.95%, accompanied by a remarkable FF of 0.847. The unencapsulated perovskite solar cell (PSC) retains 93% of its original efficiency after 1,056 h of storage and retains 91% of its initial

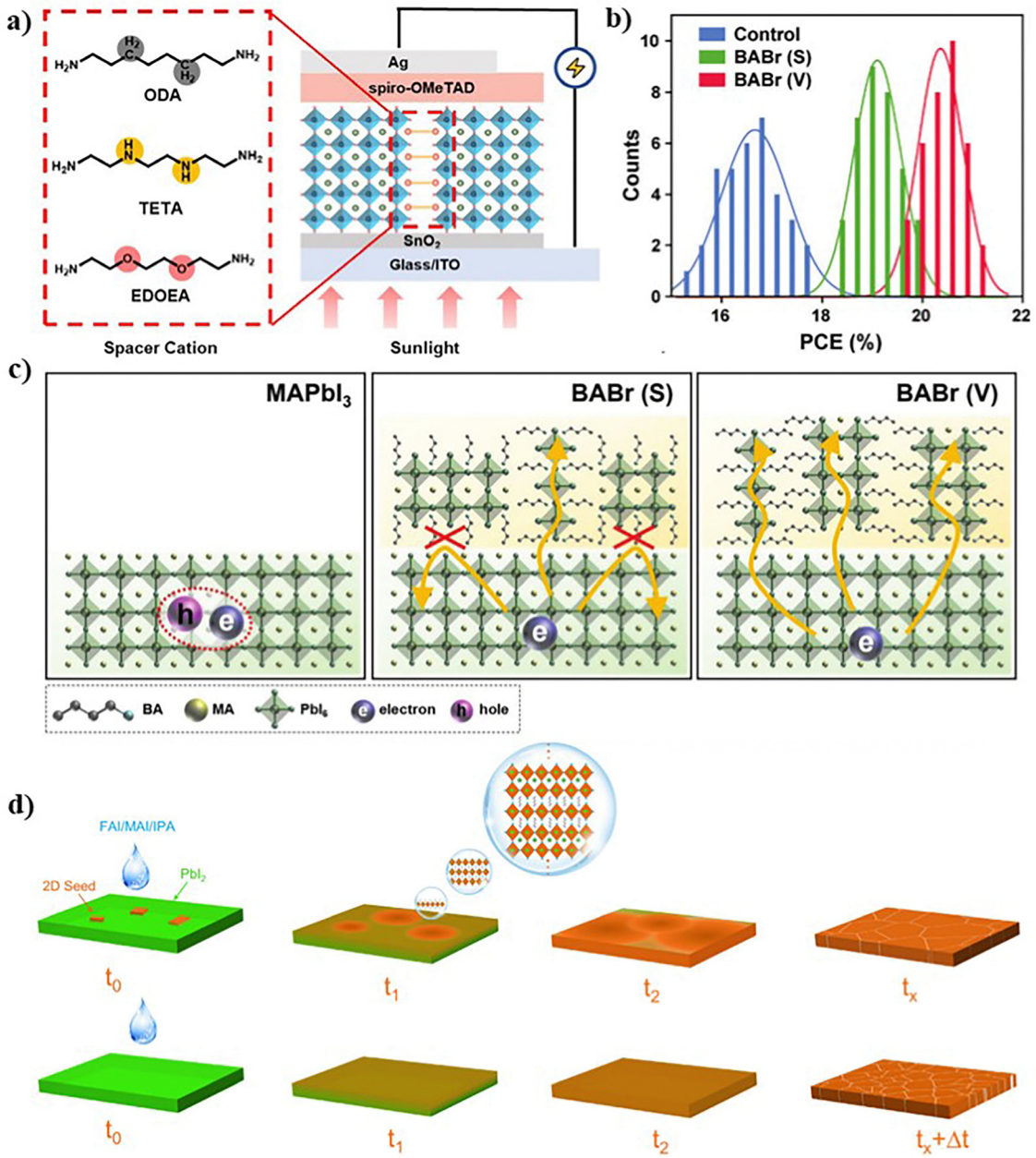

Fig. 5 (a) Device structure and molecule structure (ODA, TETA and EDOEA) of 2D/3D perovskite solar cells.[79] Schematic of (b) PCE distributions and (c) the perovskite crystal structure and charge transport for control, BABr (S), and BABr (V) films.[80] (d) Schematic diagram of film growth 2D-seed-induced and without 2D seeds.[81]

efficiency after 500 h of operation at the MPP under simulated AM1.5 illumination at 60 °C. Zhao *et al.* also found the seeds, with different n values (n = 1, 2, 3, and 4), had almost no obvious effect on the photovoltaic performance of PSCs. In addition, a flexible PSC with a PCE of more than 20% and DJ phase (3AMP)PbI_4 as seeds with a PCE of 23.5% was obtained, indicating the versatility of 2D-seed-induced growth.[81]

2.2.4. Polarity design of 2D layers. Appropriately designed electronic polarity (such as ferroelectricity, polarity, electron donating groups, *etc.*) can facilitate the charge transfer across a 2D/3D perovskite interface. Recently, Han *et al.* uncovered that incorporation of a ferroelectric 2D material based on a pyridine heterocyclic ring as the organic interlayer into a 3D perovskite induces an increased built-in electric field, which enhances the exciton dissociation efficiency in the device. This ferroelectric 2D seeds could assist the 3D crystallization by forming more homogeneous and highly oriented perovskite crystals (Fig. 6a). As a result, an impressive power conversion efficiency (PCE) over 23% has been achieved by the f-PSCs with outstanding ambient stability.[83]

The addition of polar materials (such as dipoles) in 2D/3D interface processing could also improve the performance of

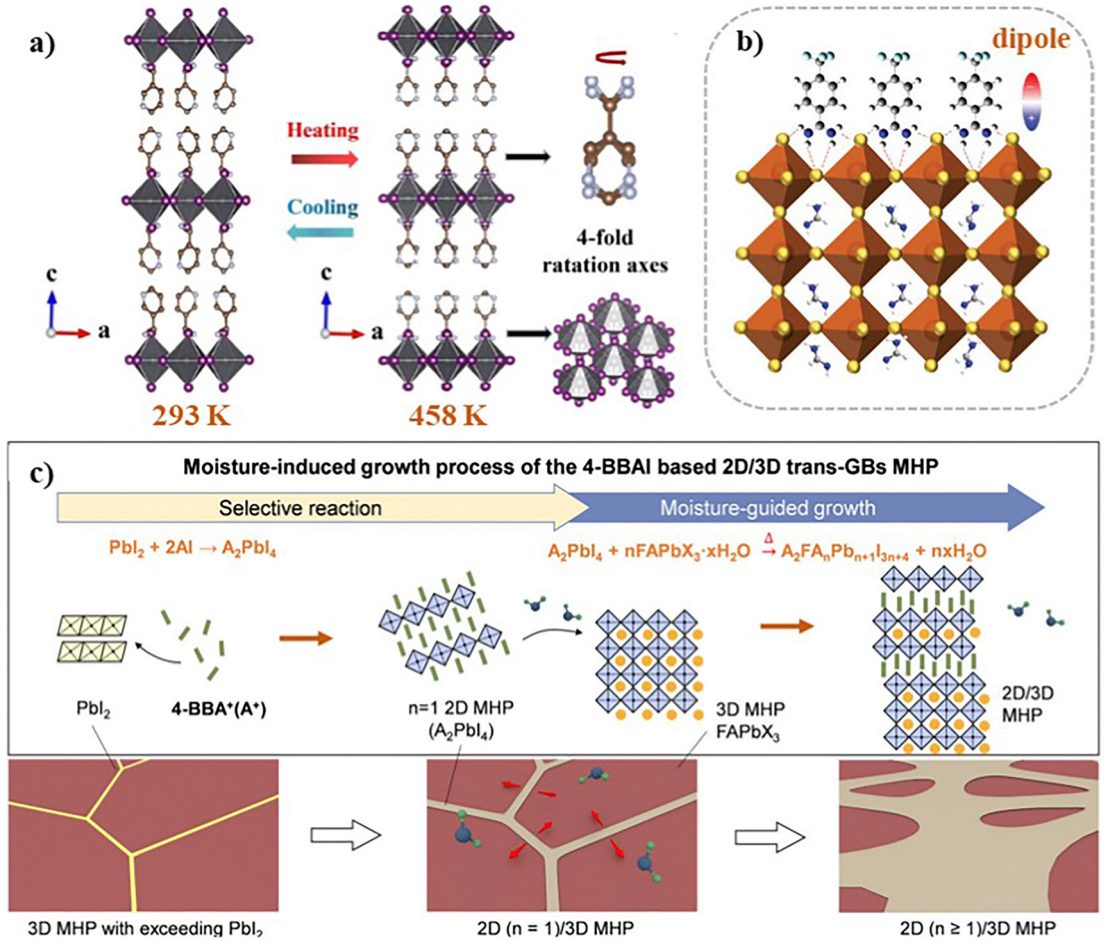

Fig. 6 (a) Crystal structures of $(3\text{-PyAI})_2PbI_4$ at 293 K and 458 K.[83] (b) Schematic diagram of the chemical interaction between $TFPhFA^+$ and the Pb-I octahedron, a unique electronic structure (dipole) brings the additional optimization effect.[84] (c) Schematic illustration of the structural evolution mechanism of 4-BBAI 2D MHP on the 3D MHP surface based on the selective chemical reaction and moisture-guided growth.[85]

PSCs. Yue *et al.* applied 4-(trifluoromethyl)benzamidine hydrochloride (TFPhFACl) as an organic spacer cation to construct a 2D perovskite on top of a 3D perovskite. The $TFPhFA^+$ layer with large polarity formed a dipole layer, which could facilitate the carrier transport. Meanwhile, these molecules could suppress the nonradiative recombination through the chemical interaction between $TFPhFA^+$ and PbI_2, and recrystallization of the 3D perovskite induced by Cl^- anions (Fig. 6b). As a result, the PCE of a PSC with TFPhFACl treatment was improved from 21.9% to 24.0% mainly due to the increase in the FF and V_{OC}. There is no decrease in efficiency for TFPhFACl treated PSCs after 1500 h storage in a dry box, indicating their good air-stability.[84] Yan *et al.* found that the mild polarity of *X*-bromobenzylamine (*X* = 2, 3, 4) salts plus the ambient moisture stimulated the growth of 2D perovskites to form a trans-GBs structure (Fig. 6c). Therefore, trans-GBs 2D/3D based flexible-PSCs exhibited a certified PCE up to 22.1% and maintained ~ 80% of their initial PCE after 8000 bending cycles (R = 4 mm).[85]

Li *et al.*[86] reported that the grain boundary and interface have been dual optimized in a 2D@3D/2D perovskite by introducing 2-(2-pyridyl)ethylamine (2-PyEA) molecules with a 2D structure and as a negative dipole for electron donating into the perovskite. As an additive, 2-PyEA promoted the generation of a 2D@3D perovskite; as a post-treated modifier, 2-PyEA facilitated the formation of a 2D@3D/2D perovskite. Based on this dual optimized strategy, crystallinity of the perovskite film was optimized with released residual stress, matched energy level, reduced defect density, and prolonged carrier lifetime. Consequently, the dual-optimized PSC achieved a maximum PCE of 23.2% with a negligible hysteresis and satisfactory stability. They also used 1,8-naphthyridine (1,8-ND) with electron-rich properties as an interfacial modification material to form effective coordination with Pb^{2+} ions and construct a stable 2D/3D interface.[87] Because of the passivated surface defects and improved hydrophobicity, the targeted devices achieved a champion PCE of 23.8% and retained 83.2% of initial PCE after 50 days of exposure in air with 30% humidity.

Constructing 2D/3D perovskite heterojunctions is effective for surface passivation of perovskite solar cells (PSCs). The interface passivation strategy of 2D materials is utilized to continuously improve the PCE of PSCs by updating the types

of materials and implementing reasonable passivation molecule design methods, such as functional group modification and *n*-value regulation.

2.3 Methods to achieve low-dimensional perovskite crystallization

In addition to constructing 2D/3D perovskite heterojunctions and employing interface passivation strategy with 2D materials, various other techniques have been developed to regulate 2D perovskites. These include the formation of low-dimensional perovskite structures, the creation of self-assembly layers, the application of small molecule permeation methods, and the implementation of multiple interface co-passivation strategies.

2.3.1. Low-dimensional control of perovskite. It has been reported that a layer of a low-dimensional (LD) perovskite could improve the performance of 3D-based PSCs effectively. In contrast to three-dimensional (3D) perovskites, low-dimensional (0–2D) perovskites show superior moisture stability due to the hydrophobicity of their large organic cations.[88,89] It could passivate the defects on the interfaces, improve carrier lifetimes, alter band alignment, prevent the penetration of water molecules into the perovskite bulk and so on.[90,91] A 2D perovskite layer was usually used to construct 2D/3D mixed structure PSCs and improve performances, but there are relatively few reports on 1D perovskites. Herein, we will discuss and compare the work based on two types of low dimensional perovskites.

To form a LD layer for high-performance devices, Hu *et al.* introduced 4-aminobutyric acid (C4I) and 6-aminocaproic acid iodides (C6I) onto the surface of a perovskite layer. They found that C4I forms a 2D perovskite layer, while C6I forms a 1D perovskite layer on a 3D perovskite surface (Fig. 7a). These low-dimension capping layers can passivate the surface defects, improve the carrier lifetimes, and alter the band alignment, leading to improved solar cell efficiencies as high as 23.48% (C4I) and 23.11% (C6I), respectively.[91] Meanwhile, Kim *et al.* investigated the effect of the chemical bonding types of the post-treatment materials on the photovoltaic performance and photoexcited carrier behavior based on two materials of PyI (pyridinium iodide) and PpI (piperidinium iodide) with geometrically similar chemical structures but distinctly different chemical bonding natures (the π orbital for PyI and the sp3 orbital for PpI in the N-bearing heterocyclic ring). They found that an insulating 1-D $PpPbI_3$ formed by PpI treatment blocks the charge separation, which is pronounced at high concentration. As a result, a monotonical increase in PCE from 20.13% to 22.26% is observed as the PyI concentration increases from 0 to 40 mM, while for PpI, the PCE is optimized at a relatively low concentration of 5 mM, which suggests that the optimal concentrations (or thicknesses) are different for each material (Fig. 7b).[92]

However, the insulated organic cations of low-dimensional perovskite impede the transport of carriers, decreasing the

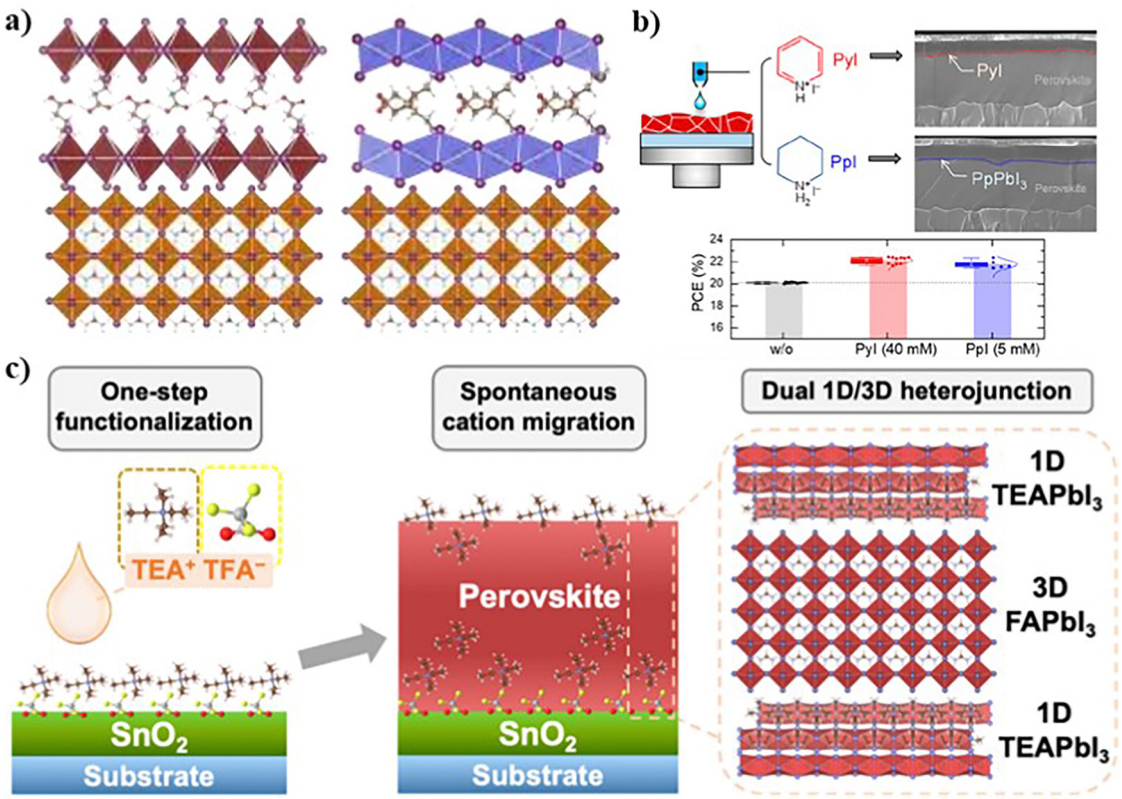

Fig. 7 (a) Dimensional regulation using the different 2D perovskite organic salt ($(HOOC(CH_2)_3NH_3)_2PbI_4$ and $(HOOC(CH_2)_5NH_3)_2PbI_4$, respectively).[91] Passivation method using (b) molecules with different chemical bonding natures (PyI and PpI)[92] and post-treatment-free dual-interface by TEATFA.[93]

power conversion efficiency (PCE) of PSCs. Yang *et al.* introduced an *in situ* cross-linking polymerizable propargyl ammonium (PA^+) to a 3D perovskite film at surfaces and grain boundaries to form a 1D/3D perovskite heterostructure. They reported that this passivation strategy significantly improves the interfacial carrier transport and releases residual tensile strain in perovskite films simultaneously. And the corresponding devices achieve a champion PCE of 21.19%, while maintaining 93% of their initial efficiency after 3055 h of continuous illumination under MPP operating conditions.[94]

Recently, low dimensional perovskites have been further explored. Wei *et al.* introduced a dual-interface passivation method without using post-treatment through the construction of buried and capped double 1D/3D heterojunctions, which is achieved through facile tetraethylammonium trifluoroacetate (TEATFA) prefunctionalization on a transport layer substrate (Fig. 7c). The functional TEATFA salt is first deposited onto the transport layer substrate and then reacts within the interface between the transport layer and the perovskite layer. Once the $FAPbI_3$ perovskite precursor solution is dripped, a portion of the TEA^+ cations spontaneously diffuse to the top surface over film crystallization. The TEATFA-based water-resistant 1D/3D $TEAPbI_3/FAPbI_3$ heterojunctions at both the buried and capped interfaces led to much better photovoltaic performance and higher operational stability, and a PCE of over 20% was achieved following the proposed route.[93] Meanwhile, Wang *et al.* developed a strategy to modify the perovskite surface by passivating the surface defects and modulating the surface electrical properties by incorporating morpholine hydriodide (MORI) and thiomorpholine hydriodide (SMORI) on the perovskite surface. Compared with the PI treatment that we previously developed, the one-dimensional (1D) perovskite capping layer derived from PI is transformed into a two-dimensional (2D) perovskite capping layer (with MORI or SMORI), achieving dimension regulation. It is shown that the 2D SMORI perovskite capping layer induces more robust surface passivation and stronger *n*-N homotype 2D/3D heterojunctions, achieving a p–i–n inverted solar cell with an efficiency of 24.55%, which retains 87.6% of its initial efficiency after 1500 h of operation at MPP.[95]

Through this work, they transformed the 1D perovskite structure into a 2D perovskite structure. And in Hu's work we mentioned before, they also showed the 2D capping was more suitable for enhancing the performance of 3D perovskites than 1D capping, which reflects the reason why researchers choose fabricating 2D layers more to improve the performance of PSCs to some extent.

2.3.2. Control of the crystallization process with a self-assembled 2D perovskite. In order to avoid additional fabrication steps to construct a perovskite film at interfaces, especially at buried interfaces, researchers developed a self-assembly strategy to form a 2D perovskite passivation layer directly at the interface. Zuo *et al.* reported a facile, spin-coating-free, directly scalable drop-cast method, in which the precursor solutions self-assemble to form highly oriented, uniform 2D-perovskite films in air, yielding perovskite solar cells with a PCE of 14.9% in 2019.[96] This self-assembling method reduced the anthropogenic nonideal factors and increased reproducibility of sample preparation. Chen *et al.* introduced an isobutyl amine (iBA) self-assembling large-*n*-value 2D perovskite (Fig. 8a) to fabricate 2D/3D perovskite films in air, realizing a champion power conversion efficiency of 18.29%.[97] Wang *et al.* added cyclohexylammonium bromide (CMABr) as a p-dopant into HTL solution to form a 3D/2D heterostructure perovskite bilayer (the buried interface is a HTL/perovskite surface in this work). Interestingly, a 3D/2D interface could be generated spontaneously without additional annealing process through the reaction between CMABr at the bottom of the HTL and the excess PbI_2 on the surface of a 3D perovskite film (Fig. 8b). They found that the exotic CMA^+ ammonium group and Br^- ions could easily insert into the ABX_3 perovskite crystal lattice to compensate A-site cation and X-site vacancies at the perovskite/HTL interface, which reduced the undesirable non-radiative recombination centers within PSCs.[98]

In addition, a self-assembly strategy can also be used in the crystallization process to improve the perovskite crystals. Chen *et al.* found that after adding thiomorpholine1,1-dioxide hydrochloride (TdCl) to the precursor solution, the colloid in the target precursor with TdCl was significantly larger (over 1000 nm) than that of conventional colloid without TdCl, which may be the pre-nucleation clusters caused by Td^+.[99] Due to the low solubility of Td^+, the preferential low-dimensional 2D Td_2PbI_4 perovskite crystals formed in solution prior to nucleation (Fig. 8c). As a result, 2D perovskite crystallite seeds in the bottom of perovskite films can be used as bottom-up templates to promote the crystal growth of 3D perovskite films, which might further improve the grain size and crystal orientation of 3D perovskites. Meanwhile, in addition to improving the crystallinity, 2D Td_2PbI_4 accumulated at the buried interface passivated the defects, lowered the carrier transport barrier and inhibited interfacial redox reactions. As a result, PSCs showed an encouraging PCE of 22.09% and high stability, retaining 85% of their original PCE after 500 h of continuous operation under MPP conditions in a N_2 atmosphere.

Meanwhile, self-assembled monolayers (SAMs) are also currently widely used structure in self-assembly methods.[100–105] The advantage of SAMs is their construction methods are independent of the 2D/3D passivation methods. The headgroups on top of SAMs can be modified to adjust their wettability and facilitate better interactions with the perovskite coated on top to passivate the interfacial defects. The more hydrophilic SAM surface can facilitate the nucleation and growth of perovskite films fabricated, forming a compact and uniform interface, especially a buried interface.[106] Recently, Tang *et al.* created an indium tin oxide substrate with a fully covalent hydroxyl-covered surface for SAM anchoring, and a SAM with a trimethoxysilane group that exhibited strong tridentate anchoring to the substrate, achieved PCE of 24.8% (certified 24.6%).[101]

2.3.3. Post treatment control with osmosis of small molecules. In addition to direct passivation in the corresponding preparation process, there are also some passivation strategies that achieve passivation by osmosis of small molecules at

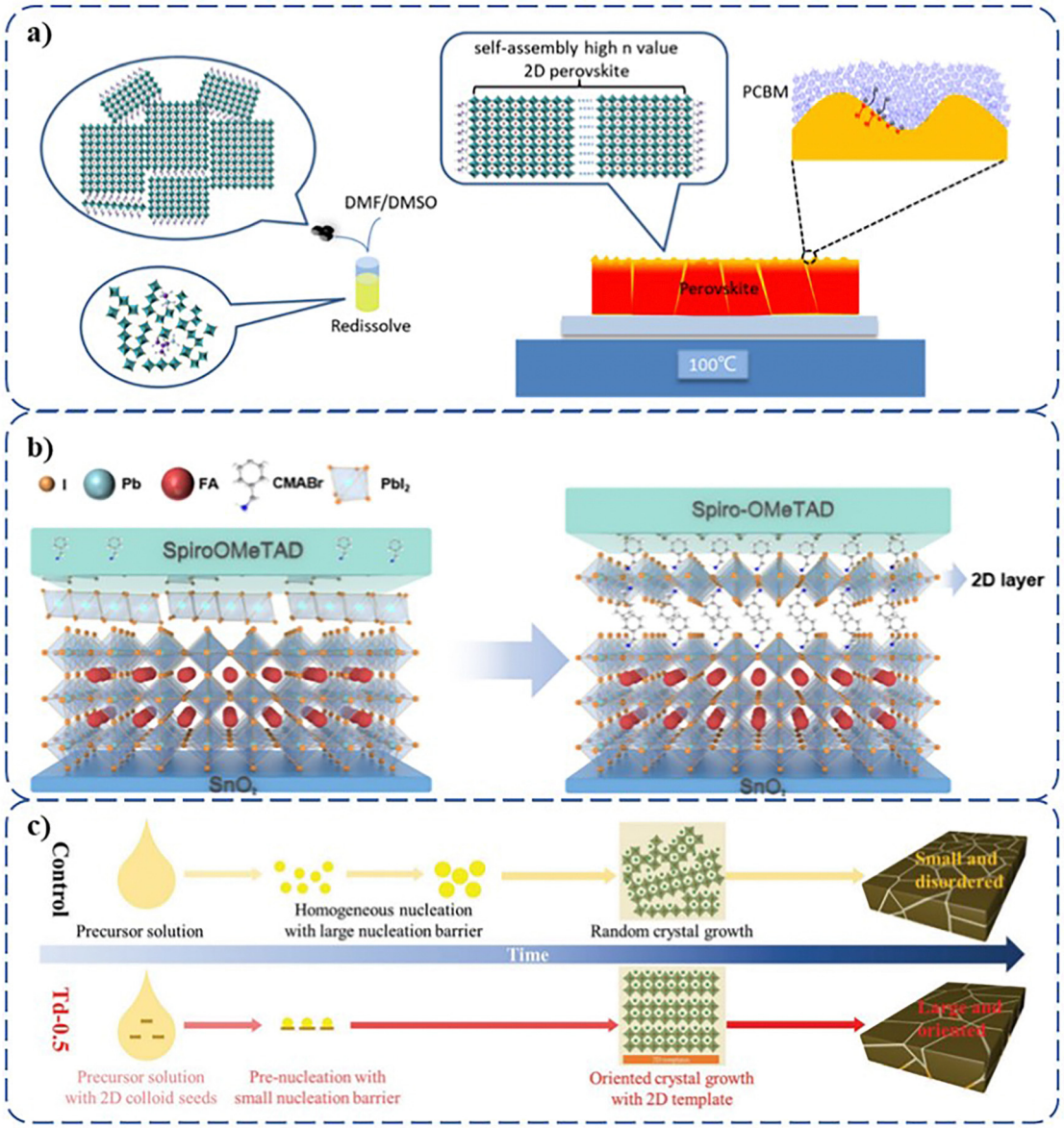

Fig. 8 (a) Schematic diagram of the protective layer of the fabricated self-assembled large-*n*-value 2D perovskite films.[97] (b) Proposed mechanism for *in-situ* formed 3D/2D perovskite heterojunctions by CMABr.[98] (c) Schematic diagram of a pre-nucleated small molecule to passivate the buried interface by Td^{+}.[99]

the interface post-treatment to form a 2D perovskite. This method is of advantage in passivating the buried surface of perovskite.

A guanidine 2D perovskite (Gu_2PbI_4) was used to passivate the buried interface, in which guanidine salt was added into the precursor solution and even post-treatment solution to realize it.[107] Chen *et al.* sought to use perovskite precursors mixed with large organic cations (including *n*-butylammonium, BA, ethylammonium, EA, dimethylammonium, DMA, and guanidinium, GUA) for the spontaneous formation of a 2D passivation layer at the buried interface. Due to the symmetry of its structure and strong bonding affinity of a cation to a substrate, only a GUA-containing precursor formed a 2D GUA_2PbI_4 buffer layer at the buried interface (Fig. 9a). The results show that the 2D interlayer suppresses non-radiative recombination at the buried perovskite/CTL interface, leading to a 72% reduction in surface recombination velocity, resulting in 22.9% PCE for 1.55 eV bandgap perovskites.[108] Zhu *et al.* reported a depth-dependent manipulation strategy to modulate the perovskite-related interface (*i.e.*, bulk, the top surface and the buried interface) defects *via* a one-step treatment with a binary mixture of guanidine iodine (GuaI) and 4-*tert*-butyl-phenylmethyl-ammonium iodide (tBPMAI). Time-of-flight secondary-ion mass spectrometry (ToF-SIMS) results confirmed that Gua could penetrate from the top surface of the perovskite bulk to the buried interface (Fig. 9b).[109]

Based on the various above methods, the passivation of 2D/3D perovskite interfaces is flourishing and continuously

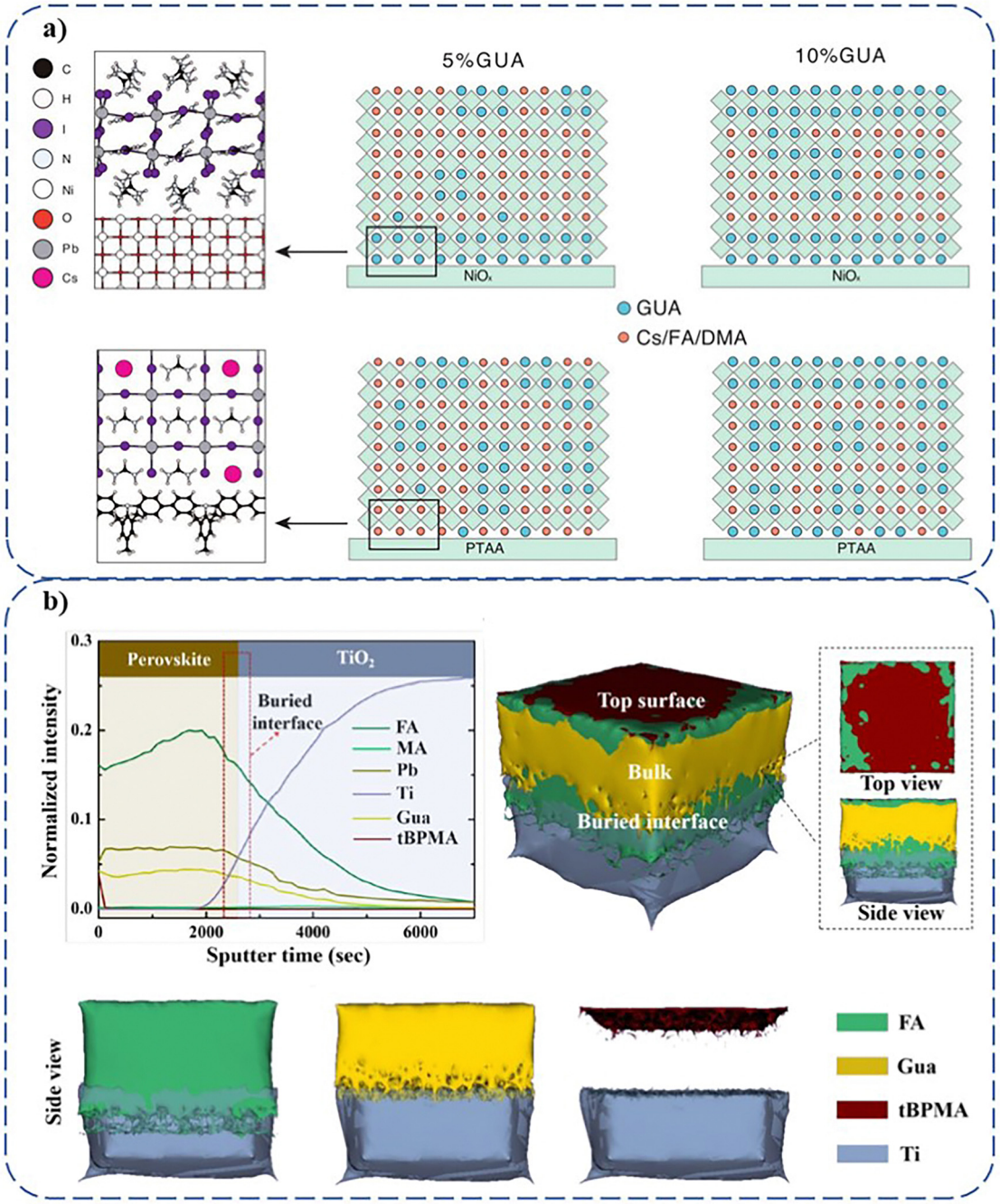

Fig. 9 (a) Mechanism of substrate-induced preferential crystallization of GUA_2PbI_4 with different GUA concentrations on NiO_x and PTAA substrates.[108] (b) ToF-SIMS depth profiles and ToF-SIMS 3D images of the binary GUAI/tBPMAI-treated perovskite film.[109]

improving *via* diverse aspects: material selection, molecular adjustment and specific strategies.

3. Interface passivation

The 2D perovskite passivation strategy is considered as a promising direction for device performance optimization. There are many high PCE works that have adopted the passivation strategy using 2D perovskites,[21,110–112] which fully prove the advantages of the 2D perovskite passivation strategy in improving efficiency and stability. In the previous section, according to different design strategies, we summarized and divided the implementation of PCE > 25% into three pathways (forming passivators, rational design and some specific crystallization methods of 2D perovskites to realize interface passivation). All these passivation strategies will work at the specific positions of PSC interfaces, to improve the efficiency and stabilization of PSCs. Herein, we investigate these strategies on three main passivation positions (buried interface, grain

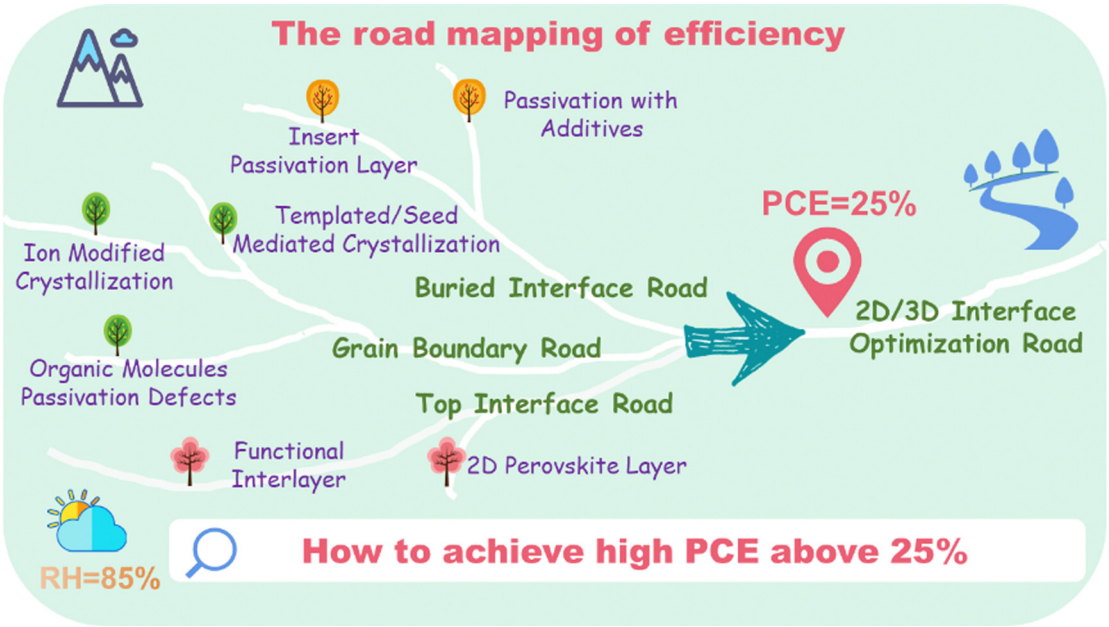

Fig. 10 The road map towards PCE above 25%.

boundary interface, and top interface) at the interface (Fig. 10). We will discuss this roadmap in detail according to the device fabrication sequence in the following sections.

3.1. Optimization of buried interfaces

In conventional n–i–p PSCs, the interface between electron transport layer (ETL) and the perovskite is usually referred to as the buried interface. In contrast, in inverted p–i–n PSCs, this term refers to the interface between the hole transport layer (HTL) and the perovskite. Due to the challenges associated with accessing and characterizing these interfaces, their interfacial properties are often overlooked. Notably, charge trap densities at grain boundaries (GBs) and interfaces were reported to be significantly higher than those within the perovskite grains.[113] In addition, both donor-type and acceptor-type defects, which are generally deep-level defects, can coexist at these buried interfaces.[114–116] These defects contribute substantially to interfacial non-radiative recombination,[117] a crucial limiting factor for the PCE of PSCs. As a result, increasing attention is being directed towards passivating these buried interfaces to enhance PSC performance. Strategies for optimizing buried interfaces can be broadly categorized into two main approaches: (1) passivation *via* introduced additives, and (2) insertion of additional passivation interlayers at the buried interface.

3.1.1. Passivation with additives. To passivate vacancies and interstitial defects in the buried interface, organic molecules with special functional groups are introduced, which improved the performance of PSCs. Yang *et al.* reported that incorporating DL-carnitine hydrochloride (DL) into a buried (perovskite/ETL) interface could reduce oxygen vacancies and interstitial tin atoms on the ETL surface and control FA^+/Pb^{2+}-related defects to achieve high performance $FACsPbI_3$ PSCs simultaneously (Fig. 11a). The DL-dimer modification effectively passivates interfacial defects and improves the quality of the resultant perovskite film, leading to a high PCE of 25.24%.[118] Furthermore, Gong *et al.* proposed a buried interface stabilization strategy that relies on the cooperation of fluorine (F) and sulfonyl (S═O). When using a series of salts containing halide and non-halogen anions (including KFSI, KTFSI, KMS and KCl) to modify an ETL (SnO_2) buried interface (Fig. 11b), the ions (anions and cations) in salts form ionic bonds with charged defects in perovskite films and passivate the positively and negatively charged defects at the same time.[114] Multiple chemical bonds including hydrogen bonds, coordination bonds and ionic bonds were constructed in this passivation method, which strengthen the interfacial contact and the defect passivation effect.

Besides being a common material for constructing a perovskite film, PbI_2 also plays a critical role in passivating the defects at the interfaces. An appropriate amount of PbI_2 in perovskite films (mainly distributed in the grain boundary) could improve the photovoltaic performance of devices, but excessive PbI_2 aggravates the instability of devices.[112,120,121] Therefore, Zhao *et al.* converted PbI_2 into an inactive $(PbI_2)_2RbCl$ compound by RbCl doping. The XRD results (Fig. 11c) and the SEM results both proved that more PbI_2 phases appeared in the samples without RbCl after the perovskite film was heated at 85 °C for 48 hours.[40] This means that compared with PbI_2, it is more difficult for $(PbI_2)_2RbCl$ to react with FA and I to cause FA and I formation, and more difficult to provide ion migration channels, thus inhibiting perovskite degradation and stabilizing the perovskite phase effectively and solving the instability problem caused by excessive PbI_2.

Recently, buried interface passivation engineering has been developed by introducing passivation additives to form co-passivation which could modify more than one interfaces in

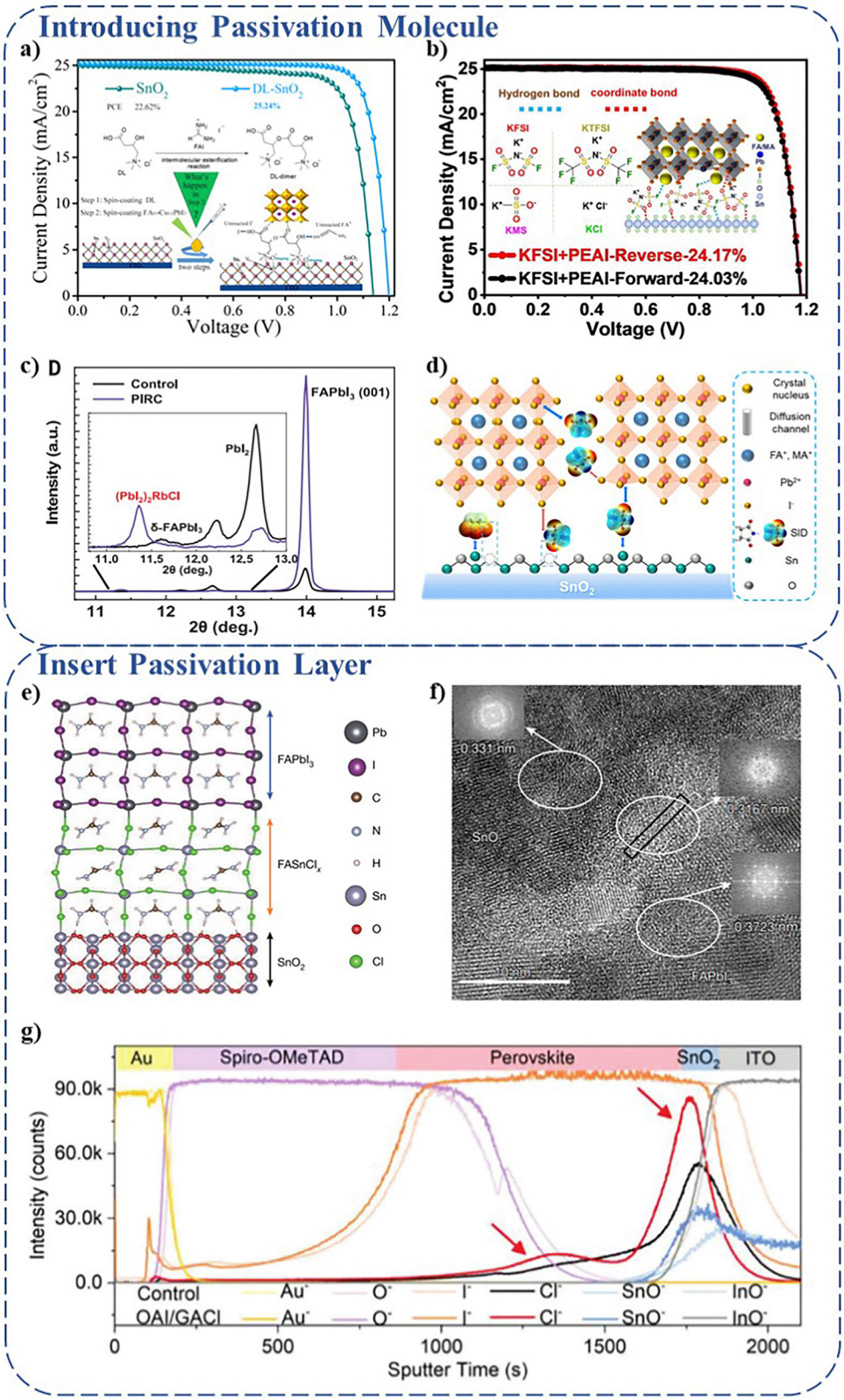

Fig. 11 Diagram of (a) DL[118] and (b) KFSI[114] interface passivation mechanism. (c) XRD patterns of perovskite without RbCl and with 5% RbCl.[40] (d) Schematic illustration of a chemical mechanism for regulating the crystallization of lead iodide films and passivating defects using SID.[119] (e) Simulation of the formation and (f) HR-TEM for the multilayers obtained from Cl-cPP on Cl-bSO.[41] (g) ToF-SIMS depth profile of a full perovskite solar cell based on the control and OAI/GACl-treated perovskite.[111]

PSCs together. Li *et al.* reported an auxiliary passivation method (Fig. 11d) for enhancing the performance of PSCs by passivating both the perovskite phase and the buried interface using succinimide (SID). They demonstrated the remarkable ability of SID to coordinate with Pb^{2+} through Lewis-base coordination and bind the iodide ion with hydrogen bonds, thereby reducing defects within the perovskite and suppressing nonradiative recombination. Additionally, SID could passivate oxygen vacancies and hydroxyl defects on the ETL surface, facilitating carrier separation and extraction. This multilayer passivation strategy enables achieving a PCE of 24.47% based on a two-step process.[119]

3.1.2. Insertion of passivation layers. In addition to introducing passivation additives, PSC performance could also be improved by introducing an interlayer to the buried interface. Buried interface passivation is more difficult to access compared to other interface passivation, because the organic passivation molecules added for surface-treatment on the buried interface may dissolve while coating the perovskite layer, resulting in a minimal passivation effect. For example, Zhou *et al.* adopted a 2D $(NpMA)_2PbI_4$ (NpMA denotes naphthalene methylammonium) perovskite to passivate the defects at the grain boundary and improve the crystallinity. But the prefabricated 2D perovskite in the buried interface has been dissolved in the second-step organic salt deposition process, and then failed to modify the buried interface.[122] If a passivation layer could be successfully formed between the transporting layer and perovskite layer without dissolution, the issue of interfacial defects may be further alleviated.

In order to completely avoid the dissolution of a predeposited 2D perovskite at the buried interface, researchers have developed a post-treatment passivation method, namely adding a passivator to the buried interface after depositing the perovskite layer. This method usually uses small molecular materials which can cross the perovskite layer as the passivator, and it is a kind of small molecule osmosis strategy. For example, Shen *et al.* applied double interactive salts of octylammonium iodide (OAI) and guanidinium chloride (GACl) onto a 3D perovskite surface, modulated the top interfaces, buried interfaces, and grain boundary interfaces (*i.e.*, grain boundaries) of the perovskite film. They found that the hydrogen-bonding interaction between OA^+ and GA^+ decelerates the OA^+ diffusion, favoring the growth of 2D perovskites with a high *n*-value ($n \geq 2$) on the 3D perovskite surface. Meanwhile, the diffusion of the smaller anions Cl^- to the buried interface of the 3D perovskite formed a chloride-rich perovskite region, and the GA^+ diffuses to the bulk crystal (Fig. 11g). These ion diffusions lowered the defect densities and further enhanced the V_{OC}, facilitating to achieve five-layer structured PSCs (n-inter-i-inter-p) with a champion PCE of 25.43% (certified 24.4%).[111]

In addition, Seok's team used Cl as a medium to construct a $FASnCl_x$ atomically interlayer at the interface between the ETL (SnO_2) and perovskite, which could improve the carrier transport capability and the efficiency of the corresponding devices[41] (Fig. 11e). From analytical characterization (HR-TEM in Fig. 11f, ToF-SIMS), they found that the crystalline $FASnCl_x$ phase formed an atomically coherent interlayer between the perovskite and SnO_2. This interlayer reduces the interfacial charge recombination loss and contact resistance, enabling PSCs with this interlayer to exhibit a PCE of 25.8% (certified 25.5%), and unencapsulated devices maintained about 90% of their initial efficiency even after continuous light exposure for 500 hours. In this work, $FASnCl_x$ interlayers have not been clearly identified as 2D perovskites. From this, it can be seen that there is still a difficulty in constructing a 2D perovskite interface passivation layer at the buried interface.

3.2 Optimization of grain boundary interfaces

Grain boundary passivation in PSCs is a crucial aspect that affects the photovoltaic performance and stability. Due to the quantum confinement effect from insulating organic components,[16,123,124] the 2D perovskites constructed for interface passivation may adversely affect the charge carrier transport, facilitate ion migration, and even produce deep sub-band energy levels within the bandgap, leading to significant nonradiative losses that limit photovoltaic performance.[125,126] Thus, in order to avoid the adverse effects of randomly distributed 2D perovskites on carrier transport and device performance, it is necessary to carefully control the morphology, grain size, preferred orientation, charge recombination, and defect density in perovskites. Various techniques have been explored to optimize the crystallization process and passivate grain boundary defects in the perovskite layer. These techniques encompass three main approaches: templated crystal or seed mediated crystallization, ion modified crystallization and organic molecule passivated defects.

3.2.1. Templated or seed mediated crystallization. Regulating the morphology of a perovskite during the crystallization process is important to obtain a high quality film with an appropriate crystal orientation and grain size. Templated crystallization and seed-mediated crystallization are two kinds of efficient methods to achieve a high quality perovskite, which could lead the crystal to exhibit a growth orientation along the specific direction with reduced defect density[127] or an accelerated crystallization rate.[81]

Seed-mediated crystallization can improve the film quality as it provides nuclei where the crystallization commences without overcoming the critical Gibbs free energy for nucleation. Zhang *et al.* reported that low-solubility ligands can be used as seeds to manipulate the nucleation and crystal growth of a perovskite during solvent evaporation (Fig. 12a).[128] And Zhao *et al.* grew a layer of a 2D perovskite seed for *in situ* epitaxial growth of a 3D perovskite on top of it, resulting in a high-quality 2D/3D heterojunction (Fig. 12b). It is found that the epitaxial 3D perovskite film exhibits a preferred [112] direction, which is different from usual perovskites with a preferred [001] orientation (Fig. 12c). The modified perovskite layer has a smooth surface, an increased grain size and fewer grain boundaries, leading to lower defect density, longer charge-carrier lifetime, better stability, and higher efficiency (24.83%).[42]

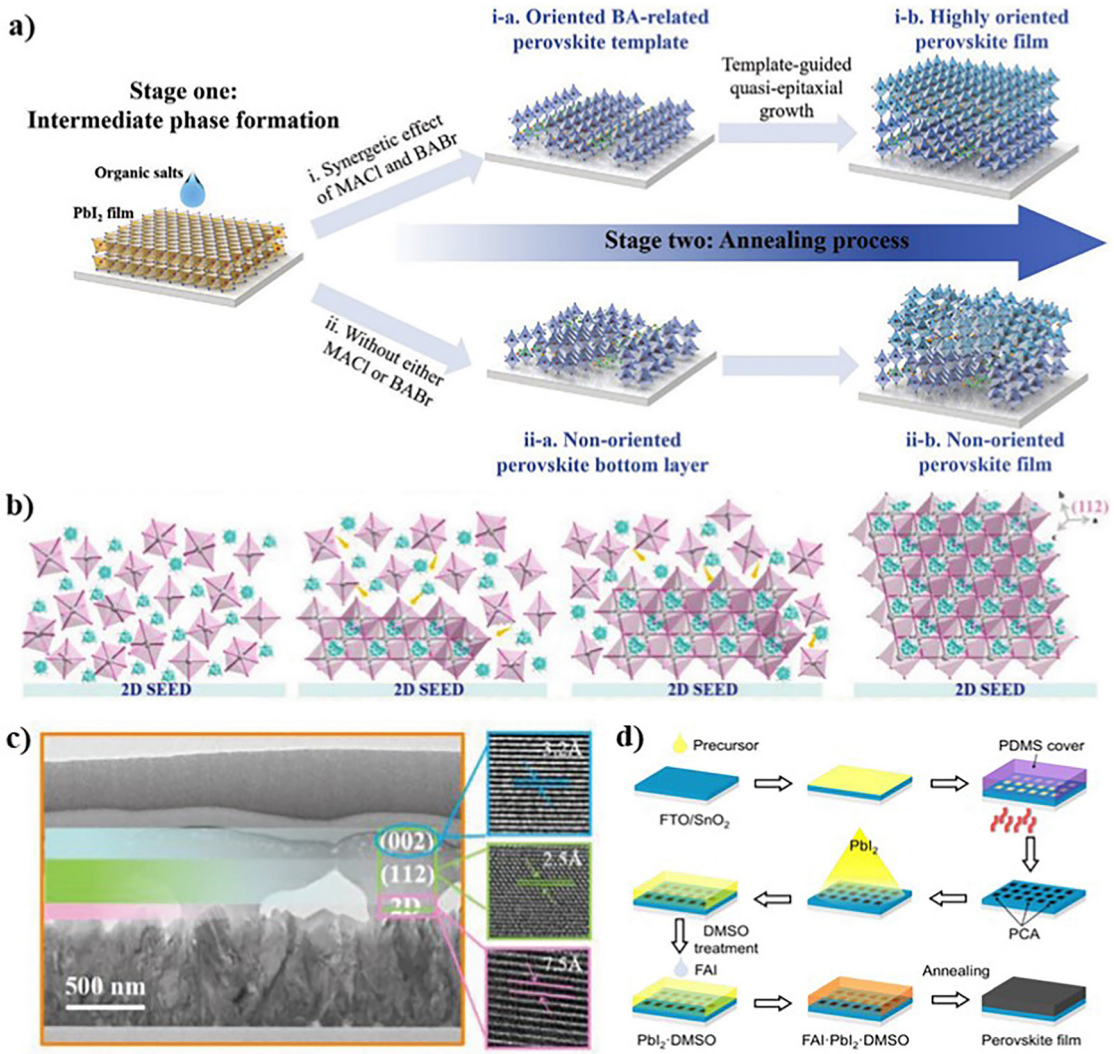

Fig. 12 (a) Schematic illustration of the bottom-up quasi-epitaxial growth of a hybrid perovskite *via* a two-step method.[128] (b) The crystallization process of the 2D-induced 3D perovskite epitaxial growth. (c) HR-TEM and FFT images of the seed-mediated perovskite film.[42] (d) Schematic description of the perovskite based on PCA-assisted growth.[129]

However, the solution-based seed-mediated method usually showed a random distributed seeds which could possibly be damaged by the subsequent solution process, limiting the controllability of the whole process. To solve this issue, a deposition method using a template layer at the buried interface to control the crystallization kinetics process of perovskite has been proposed. Shen *et al.* proposed a strategy, which uses a prepared patterned perovskite crystal array (PCA) as a templated crystal, to realize a high-quality perovskite film whose average grain size is over 3 μm (Fig. 12d). The PCA provides nuclei where the crystallization can commence without overcoming the critical Gibbs free energy for nucleation and induces a controllable bottom-up crystallization process under solvent annealing. Thus, the devices achieved a PCE of 25.1% (certified 24.3%) with an aperture area of 0.0784 cm^2 and 23.1% (certified 22.3%) with an aperture area of over 1 cm^2.[129]

3.2.2. Ion modified crystallization. In addition to controlling the crystallization process by kinetics, adding appropriate ions can also affect the crystallinity, crystal structure and grain orientation of the perovskite layer, and the passivation of defects at grain boundaries.

On the one hand, introducing long chain cations (2D) could control the crystallization process, and form a 2D/3D heterojunction simultaneously. Recently, Yang *et al.* first designed a 2D/3D heterostructure composed of a $FAPbI_3$-based 3D perovskite and an amidino-based DJ-type 2D perovskite ($(4AP)PbI_4$, 4AP = 4-amidinopyridine) (Fig. 13a).[130] The 2D perovskite assisted the nucleation of 3D perovskite during spin coating, followed by thermal annealing through *in situ* optical diagnostics, which decreases concentrations of voids and bulk defects of perovskite films for efficient charge transport (Fig. 13b). Devices based on 2D/3D heterostructures deliver PCEs of up to 24.9% on rigid substrates and 22.3% on flexible substrates. For rigid solar cells without encapsulation, 97% of original efficiency was retained after 1000 hours of ambient storage (30–40% RH), and 92% for flexible solar cells after 3000 bending

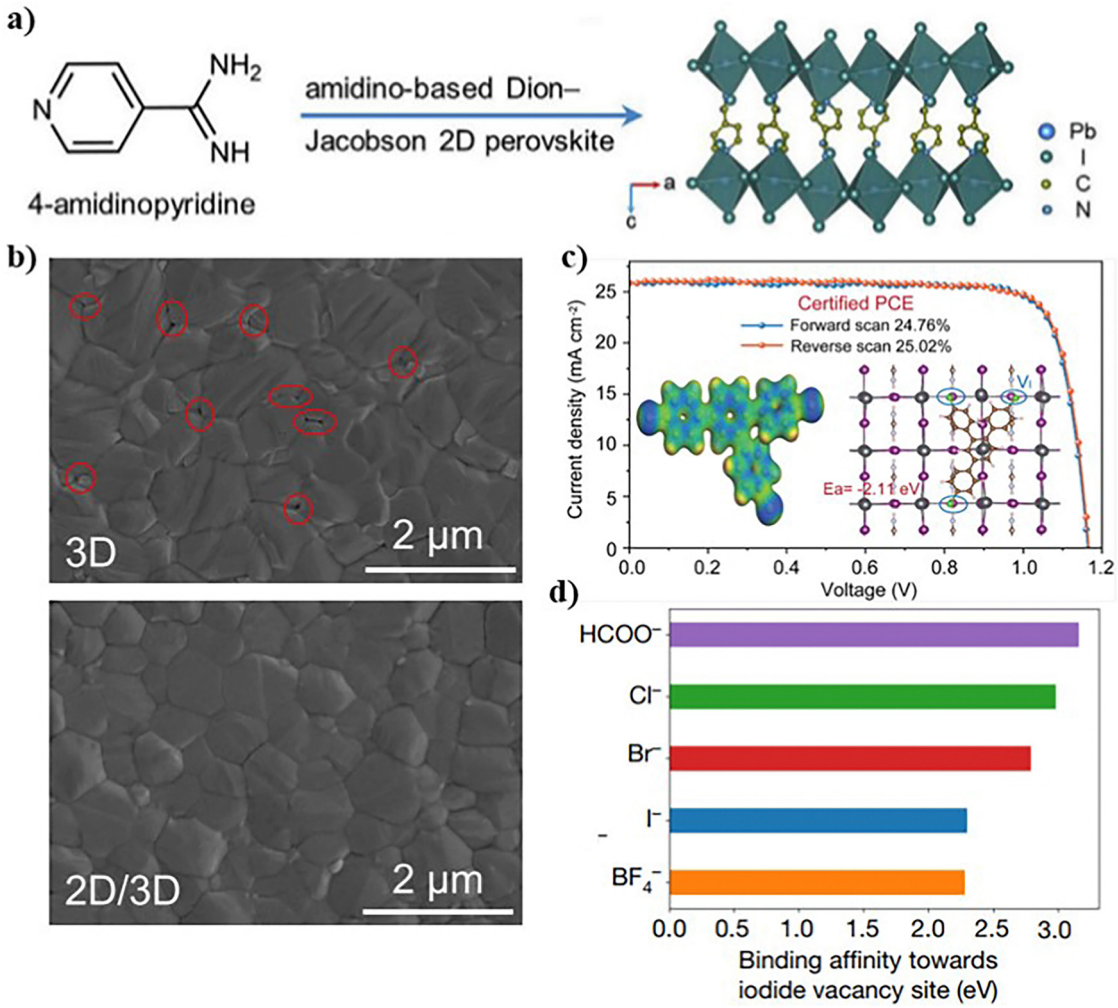

Fig. 13 (a) Molecular and crystal structures of (4AP)PbI_4, and (b) SEM surface images, the grains became more compact by adding 2D perovskites.[130] (c) Schematic illustration of a passivation strategy using atomic-Cl containing organic molecules.[43] (d) Binding affinity of different anion passivated iodide vacancies in the $HCOO^-$ passivation strategy.[44]

cycles. Meanwhile, Fang *et al.* reported a generic pre-annealing treatment for reconstructing sequentially deposited perovskite crystallites and GBs by OACl. Specifically, they treated the perovskite upper surface with OACl prior to annealing of the perovskite film, so that OA^+ of the perovskite was deposited on the grain boundary of the perovskite, and PbI_2 was transferred from the grain boundary to the top interface. With this strategy, robust GBs are created *via* defect suppression with preferred oriented large perovskite grains. As a result, the OACl pre-annealing treated devices yielded a PCE of nearly 25% with an extremely high FF of 85.5%.[131] However, it should be noted that despite the widespread use of 2D/3D heterostructures to augment device stability or performance, the location where nucleation/growth begins and the influence of the addition of 2D perovskites on the crystallization pathway of 3D perovskites have not been completely explored yet.[132,133]

On the other hand, the anions also affect the crystallization. Chloride ions are the most common additive agents which could regulate crystallization through volatilization. According to Seok group's work,[110] Cl^- of different ammonium salts (such as MACl, BACl, and PACl) could interact with PbI_2 to form intermediates, making it more inclined to form an octahedral structure of PbI_6, which affected the transformation of the δ into α phase and improved the quality of perovskite films. Meanwhile, Wu *et al.* reported a passivation strategy using atomic-Cl containing organic molecules with a large radius instead of the widely used ionic-Cl salts, which were prone to incorporate into the perovskite lattice and distort the lead halide octahedron, resulting in degraded photovoltaic performance.[43] This strategy can efficiently passivate surface defects *via* strong Pb–Cl bonding while preventing the Cl incorporation into the perovskite lattice through the strong covalent bonding between Cl atoms and organic frameworks in molecules (Fig. 13c). They investigated the relationship between passivation effectiveness and molecular configuration *via* regulating the spatial position of Cl in organic frameworks. They found that only when the distance of Cl atoms in single molecules matches the distance of halide ions in perovskites, maximized

surface defect passivation is achieved. Using this optimal configuration of Cl atom-containing organic molecules, they achieved a certified PCE of 25.02% for PSCs which can retain 90% of their initial PCE after 500 h of continuous operation.

Aside from chloride ions, there are other anions that could be used to modify the grain boundary interfaces of perovskite layers. Kim *et al.* used the pseudo-halide anion formate ($HCOO^-$) to suppress anion-vacancy defects that are present at grain boundaries and at the surface of the perovskite films and to augment the crystallinity of the films. Molecular dynamics simulations illustrate that the $HCOO^-$ anion, which has higher binding energy to V_I than other anions (Cl^-, Br^-, I^- and $BF4^-$), is more effective to passivate the V_I^- defects (Fig. 13d). In addition, the FA^+ cations at the interface also form stronger bonds with $HCOO^-$ than with other anions in this work, which thereby suppresses the FA^+ volatilization. The resulting PSCs attained a PCE of 25.6% (certified 25.2%) and a long-term operational stability (450 hours).[44]

3.2.3. Passivation of defects using organic molecules. Besides the crystallization process control and crystallization modification by ions, introducing organic molecules to passivate through stress relief, phase segregation inhibition, defect passivation, and other pathways is also a critical strategy to improve the performance of PSCs. Min *et al.* reported that trioctylphosphine (TOP) as a neutral ligand was introduced in $FAPbI_3$ solution, which relieved the preferred orientation issue, induced a redshift of the band gap through the reduction of microstrain and suppressed the defects by passivating the surface termination of grain boundaries, thus achieving an efficiency close to 25%.[45] Meanwhile, Li *et al.* inserted homogenous $CsPbBr_3$ crystals into the $FAPbI_3$ perovskite to tailor the crystallinity and defects, leading to a phase-pure $FAPbI_3$ with an enlarged grain size and also improved crystal orientation uniformity and diminished deep-level defect densities. As a result, the champion PSCs exhibited a PCE of 25.09% (certified 24.66%), with a record FF of 86.9%.[134]

Phase segregation inhibition is another kind of modification method. Shi *et al.* proposed a method for *in situ* grain boundary passivation in PSCs by introducing 3,4,5-trifluoroaniline iodide (TFAI) into the perovskite precursor to address energy loss in grain boundaries. They found the TFAI triggers the combination of nano-sized colloids into microclusters and facilitates the complete phase transition of α-$FAPbI_3$ at room temperature. The strong steric hindrance spontaneously fixes the TFAI at perovskite grain boundaries and suppresses defects there (Fig. 14a). The TFAI-incorporated device achieved a champion PCE of 24.81% finally, showing almost no decay over 280 h testing without pre-processing.[135]

Defect passivation is also an efficient way to passivate the grain boundary interface. In the perovskite layer of PSCs, undercoordinated Pb^{2+} was a common deep-level defect, which leads to severely nonradiative recombination loss. Thus, excess PbI_2 was introduced into perovskite precursor solutions to passivate grain boundary defects effectively in many studies on high-efficiency PSCs.[137–141] Recently, Xie *et al.* utilized a deformable coumarin as an additive for a formamidinium–cesium (FA–Cs) perovskite, which passivated Pb^{2+}, iodine, and organic cation defects during the perovskite annealing process, achieving a high PCE of over 24%.[142] Wang *et al.*[143] introduced an aromatic zwitterion of 1-(3-sulfopropyl) pyridinium hydroxide inner salt (SPHI) into a perovskite precursor to improve the film quality *via* regulating the crystal growth, and suppressing the charged defects (undercoordinated Pb^{2+} and FA vacancies) *via* coordination and electrostatic interactions from the sulfonic group and pyridine N^+ in SPHI (Fig. 14b), and achieved a champion device with a high PCE of 25.01% (certified 24.60%) along with the highest J_{SC} of 25.7 mA cm^{-2} for Br-free RbCsFAMA quadruple cation PSCs.

Meanwhile, passivation of iodine defects at grain boundary interfaces could improve the stability of PSCs.[144] Li's group found that 3-amidinopyridine (3AP) molecules (Fig. 14c) could form strong chemical bonds with the Pb–I framework to fix anions effectively, which increased the energy barrier of the formation and migration of anion vacancies. Density functional theory (DFT) results illustrate that after the addition of 3AP molecules the formation energy of I^- vacancies further increased from 1.42 eV to 3.812 eV and the migration barrier energy of I^- vacancies increased from 0.737 to 1.467 eV. The resultant devices exhibited a PCE as high as 25.3% (certified 24.8%). And the device with encapsulation retained 95% of its initial efficiency after >500 h working at the MPP under continuous light irradiation and under ambient conditions.[145] Wu *et al.* introduced fluoro-*N*,*N*,*N*′′,*N*′′-tetramethylformamidinium hexafluorophosphate (TFFH) into a ($FAPbI_3$)-based perovskite. The results show that TFFH could effectively inhibit the oxidation of I^- while also reducing the newly generated I^0 to I^-, weakening the negative effects caused by iodine vacancy defects.[136] It also formed a strong $FA^+\cdots$TFFH$\cdots$Pb–I interaction, which has a favorable impact on the perovskite crystallization dynamics and *in situ* passivation during crystallization, leading to larger perovskite grain sizes, better crystal orientation, fewer defects, and more efficient charge extraction in PSCs, as shown in the SEM images (Fig. 14d and e).

3.3 Passivation of the top interface

Due to the high ionic properties of perovskite materials, even stable polycrystalline perovskites devices tend to deteriorate when exposed to unstable environments.[146] Thus, various interface passivators have been developed to improve the device stability and efficiency of PSCs. Among these methods, top interface passivation is the most accessible and frequently employed. Many studies have demonstrated continuous improvements in device performance through the passivation of top interface defects, including post-treatment strategies.[111] In this section, we review recent advancements in top interface passivation, categorizing them into two main approaches based on their methodologies and effectiveness.

3.3.1. Functional interlayers. The first strategy to optimize the top interface is introducing functional interlayers after the formation of a perovskite layer through post-treatment. Metal oxides, polymers, molecules, or organic halides have been selected as functional interlayers.

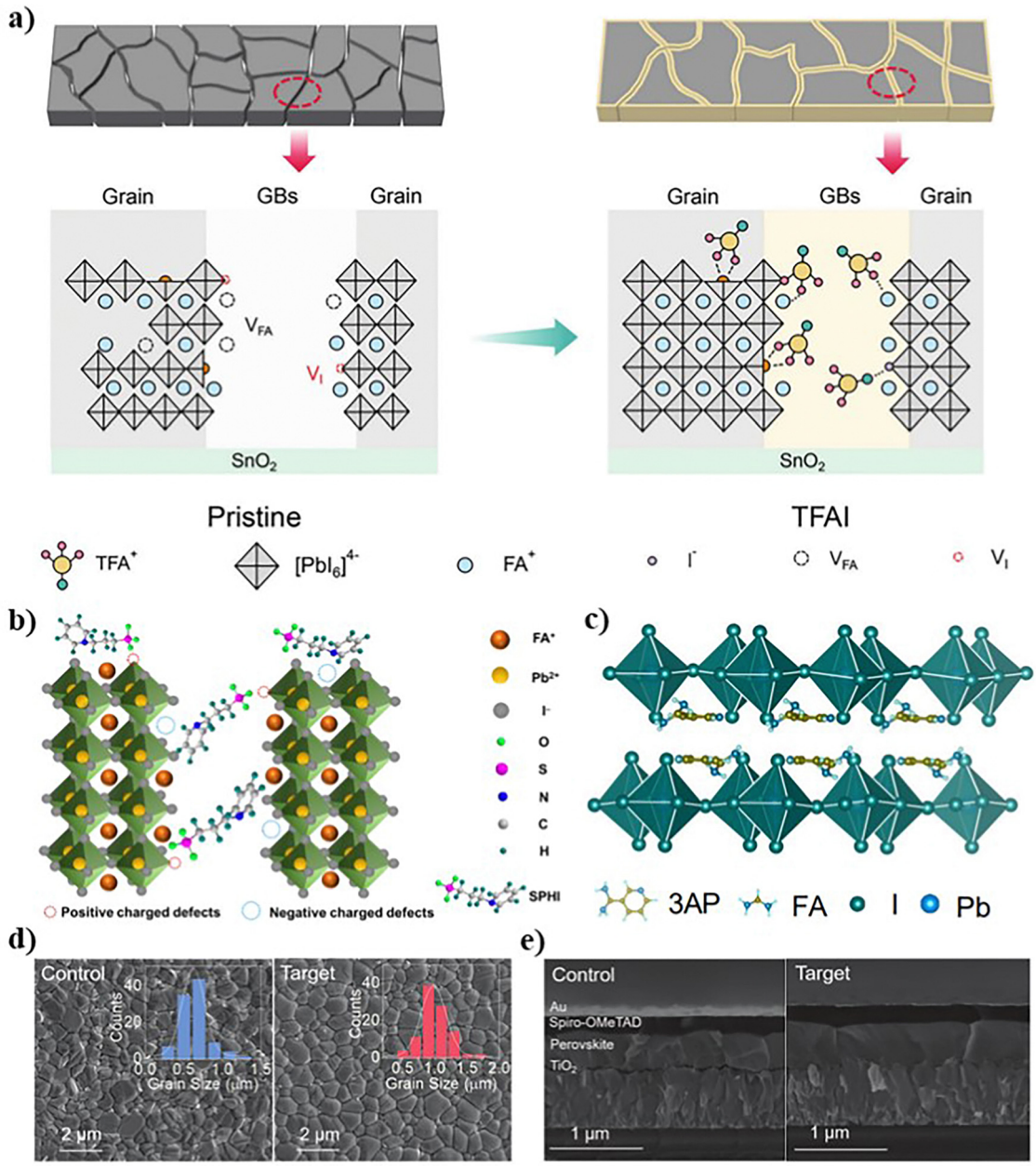

Fig. 14 Schematic diagram of the passivation strategy mechanism of organic molecules (a) TFAI, (b) SPHI zwitterions, and (c) (3AP) PbI_4. (d) Plan-view SEM and (e) cross-sectional SEM images of complete devices for both control and target films.[136]

At the interface of PSCs, defects are one of the most primary issues which impact the efficiency and stability and should be taken seriously. Among all the defects, the most common point defects in PSCs are defects of lead and iodine. In the previous section, we mentioned that PbI_2 on the top interface could suppress the defect formation.[137–141] These defects could also be solved by forming an organometallic compound layer, such as ferrocenyl-bis-thiophene-2-carboxylate ($FcTc_2$) and 3-(aminomethyl)-pyridine (3-APy).

Zhu *et al.*[147] reported that a functional interlayer formed by an organometallic compound, ferrocenyl-bis-thiophene-2-carboxylate ($FcTc_2$) on the multi-cation and halide perovskite interfaces, exhibited an enhanced PCE of 25.0% (certified 24.3%), with an increased V_{OC} of 1.184 V, a J_{SC} of 25.68 mA cm^{-2}, and an FF of 82.32% with an ignored hysteresis. DFT calculation results showed that the oxygen in $FcTc_2$ can form a strong bond with lead of the perovskite, thus passivating the surface defects of the perovskite (Fig. 15a). The insertion of $FcTc_2$ could effectively inhibit the migration and even break away the volatile components (MA) from the perovskite under continuous light conditions of 85 °C for 1000 hours, thus suppressing the degradation of the perovskite. Therefore, $FcTc_2$-optimized PSCs still maintained 98% of the initial efficiency after 1500 hours of operation at the MPP and 95% after 1000 h under the dual 85 test conditions.

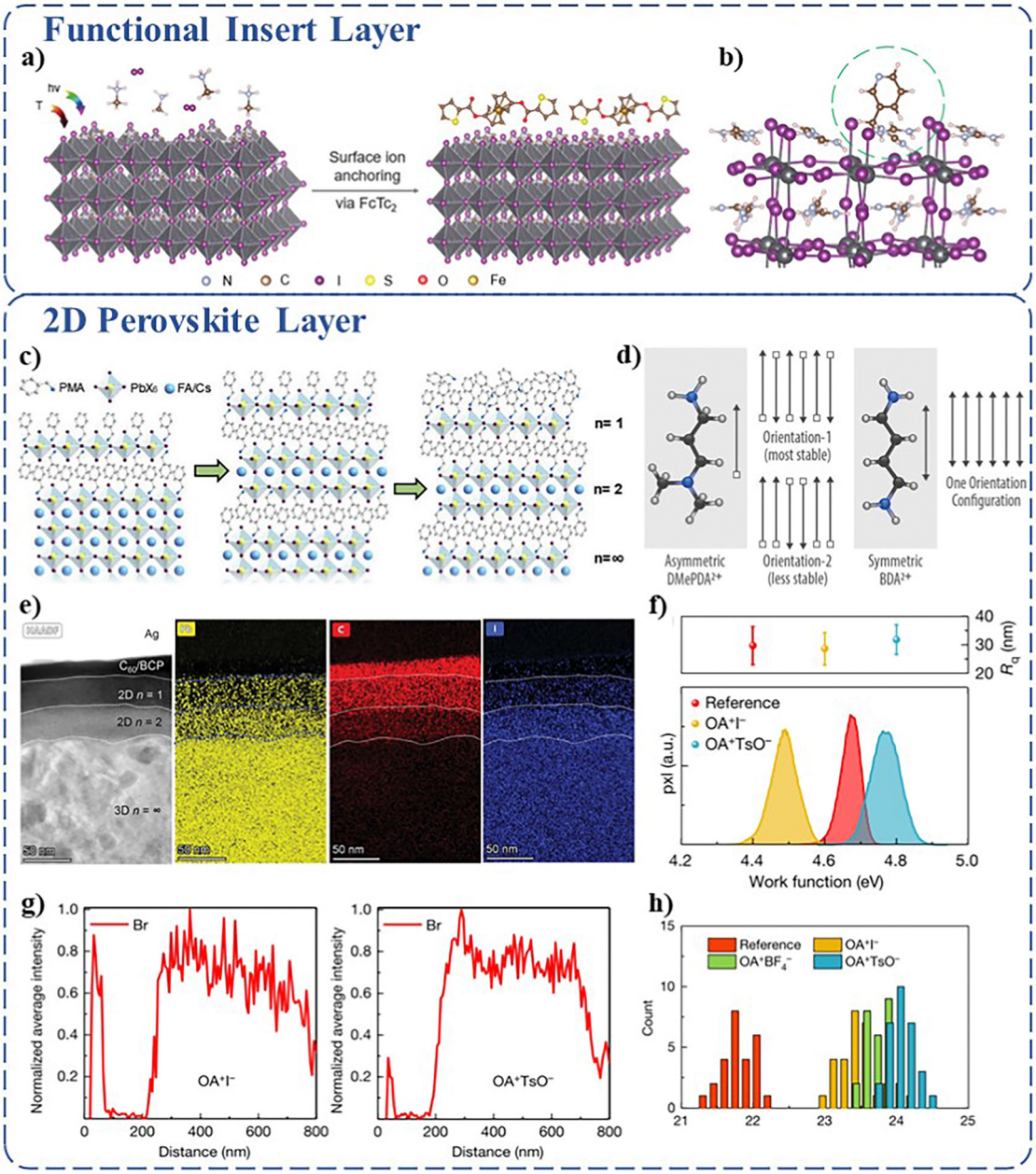

Fig. 15 (a) Schematic illustration of the stabilization of surface ions by $FcTc_2$.[147] (b) Schematic illustration of the interface modified by 3-APy.[112] (c) Schematic perovskite structure treated with low, medium or high concentrations of the PMABr/IPA solution.[148] (d) Two possible arrangements of asymmetric $DMePDA^{2+}$ and the sole arrangement of asymmetric BDA^{+}.[149] (e) Cross-sectional HR-STEM image and energy-dispersive x-ray spectroscopy elemental map of the cross-sectional STEM image of the 2D-RT samples.[31] (f) Work function distributions and root-mean-square surface roughness (R_q) of the films measured by KPFM and AFM, (g) elemental distributions of bromine, and (h) the PCE distributions of the devices obtained with OA^{+} and TSO^{-} passivation strategy.[150]

Meanwhile, Zhu *et al.*[112] demonstrated a simple post-growth treatment of 3-APy on the top interface of perovskite films. 3-APy molecules were used to reduce surfaces roughness and surface potential fluctuations associated with steps and terraces on perovskites by selectively interacting with FA^{+} ions on the surface. Consequently, the formation energy of charged V_I^{+} is reduced, leading to an effective n-type doping and a reduced work function on the surface (Fig. 15b). Benefitting from this reactive surface engineering, the optimized inverted PSCs exhibited a PCE of 25.35%, along with retention of 87% of the initial PCE after over 2400 hours under 1-sun operation and at about 55 °C in air.

Similarly, many works reported on fabrication of a 2D perovskite layer at the top interface intentionally or unintentionally, to achieve passivation and improve the efficiency and stability of PSCs. Chen *et al.* demonstrated that the reaction of a 3D perovskite with 1,4-butanediamine iodide ($BEAI_2$) vapor promotes the crystallization of the perovskite film with a large

grain size (~500 nm), resulting in efficient and stable PSCs. And interestingly, the formation of a 2D perovskite on the top interface is proved *via* XRD results. The devices fabricated with the obtained 2D/3D structure exhibited a PCE of 19.58% (compared to 17.93% of the control group).[27]

3.3.2. 2D perovskite layers. 2D perovskites are also promising materials to realize top interface passivation. The performance of PSCs could be adjusted by controlling the structure and thickness of the 2D perovskites. Bu *et al.* introduced phenylmethylamine bromide (PMABr) to modify $FA_{0.8}Cs_{0.2}Pb(I_{0.7}Br_{0.3})_3$ perovskite films, and investigated structure engineering of hierarchical layered perovskite interfaces (Fig. 15c). And they found that the structure of the 2D layer at the surface depended on the concentration of the PMABr solution.[148] With the development of constructing 2D/3D structures for top interface passivation, researchers utilized different types of passivators and methods to achieve different structures of 2D perovskite layers. Especially the two common types of 2D perovskite, ''Dion–Jacobson'' and ''Ruddlesden–Popper'' types, are often applied for top interface passivation.

Zhu *et al.* reported that a layer of metastable 2D DJ DMePDAPbI_4 perovskite was formed on the surface of the perovskite, and the 2D perovskite orientation arrangement was regulated by the asymmetry of block organic molecules (Fig. 15d), thus reducing the barrier at the interface of perovskite/hole transport layer and promoting the hole transport. Accordingly, for a triple cation-mixed-halide PSC, PCE reached 24.7% and 90% of the initial PCE was retained after 1000-hours of 1-sun operation at ~40 °C in N_2.[149] And Wolf *et al.* reported that the surface of a 3D perovskite was treated with a layer of olamiodide (OLAI), which was used to form a 2D perovskite with an RP structure, and the *n* value of the 2D layer was controlled by annealing temperature. The 2D layer annealed at 100 °C (2D-TA) tends to form a structure of $n = 1$, while the unannealed 2D layer (2D-RT) forms a mixed structure of $n = 1$ and $n = 2$ (Fig. 15e). Both 2D treatment can shift the Fermi level of the perovskite. And the 2D-RT sample's conduction band was closer to the C60 conduction band than that of 2D-TA, which led to more efficient carrier transport. The device based on unannealed 2D treatment exhibited a PCE of 24.3%, compared with 22.8% of the 2D-TA sample, which also implies that 2D layer *n*-value distribution could significantly affect device's performance.[31]

2D perovskite top surface defect passivation could also affect the heterointerface energetics. Tan *et al.*[150] found that using ammonium iodide salts (such as butanium iodide BAI, octylium iodide OAI, dodeconium iodide DAI, *etc.*) to passivate a perovskite surface could generate a reduced work function, which made the perovskite surface a n-type semiconductor. Furthermore, with the increase of the carbon chain, the work function would decrease even more (DAI > OAI > BAI). When the cation OA^+ was retained unchanged and I^- was replaced with other anions (such as Br^-, TFA^- trifluoroacetate, BF_4^- tetrafluoroborate, TsO^- benzenesulfonic acid, *etc.*), the reduction of perovskite work function was relieved (Fig. 15f), which was attributed to the stronger electron-absorbing ability of these anions, which would make it more difficult for electrons to accumulate on the perovskite surface. Among them, TsO^- can even increase the work function of a perovskite (p-type), which facilitates the transfer of charge carriers at the interface (perovskite/spiro) (Fig. 15g). PSCs after the OATsO treatment exhibited a PCE of 24.41% with a significant reduction in hysteresis (Fig. 15h). In addition, the devices passivated by OATsO had no obvious degradation after 800 h at the MPP. Meanwhile, they maintained 94.9% and 88.5% of the initial efficiency after 1014 h and 2092 h, respectively, under the open-circuit and light-soaking conditions.

The reviewed critical materials in the interface passivation section, along with their benefits, structures, photovoltaic parameters and stability properties are summarized in Table 1. After reviewing recently published works reporting high PCEs (close to or greater than 25%), we found that these works are mostly focused on passivating the three main interfaces, suggesting that interface engineering has become the most important strategy in optimizing the PSC performance. Among all of these works, the formation of 2D/3D perovskite heterostructures was becoming a common strategy for passivating interface defects of perovskites recently, so we hoped to summarize the recent work on two-dimensional perovskites for passivating three-dimensional perovskite interfaces to explore the future development direction of 2D/3D perovskites.

In addition to passivating the three main interfaces individually, some works attempt to passivate more than one interfaces simultaneously by adding the same or different passivators. Recently, Luo *et al.* proposed Cl_2-dissolved chloroform as a multifunctional solvent, and constructed a 2D/3D perovskite heterojunction on the top interface and induced the secondary growth of the bulk grains at the same time. The generated Cl^- further diffuses to passivate the bulk crystal and the buried interface of PSCs, simultaneously passivating three interfaces.[151] Similarly, Wang *et al.* proposed the use of a multifunctional molecule, α-amino-γ-butyrolactone (ABL), as a modulator to simultaneously enhance crystallization and passivate defects, improving film quality and reducing recombination losses.[152] Wang *et al.* proposed a synergetic co-modulation and co-passivation strategy by adding 4-fluoro-phenethylammonium iodide (4F-PEAI) in the precursor solution and adding poly(9-vinylcarbazole) (PVK) in an antisolvent to simultaneously enhance crystallinity and passivate the grain boundaries and surface defects.[153] Phenethyl ammonium chloride (PEACl) was incorporated into the perovskite precursor solution and PEACl surface treatment was carried out to simultaneously passivate defects at the perovskite/C60 interface as well as in the grain boundaries, which increased the charge carrier lifetime and activation energy for ion migration.[154]

Overall, these works highlight the importance of defect passivation in enhancing the performance and stability of perovskite solar cells. Various passivation materials and strategies have been explored to reduce recombination losses, improve carrier transfer, and enhance efficiency in PSCs. Future research in this area may continue to focus on developing new compositions, processing methods, and passivation techniques to further advance the field of PSCs.

Table 1 Summary of the critical breakthroughs achieved for high efficiency PSCs (approximately 25%), including passivation materials, PSC structures, photovoltaic parameters and stability

Position	Passivation material	Perovskite material	J_{SC}	V_{OC} (V)	FF	PCE (%)	Control PCE (%)	Stability (PCE retention, lifetime, and work conditions)	Ref.
Buried interface	TA	$FA_{0.92}MA_{0.08}PbI_3$	25.43	1.174	83.1	24.81	23.04	95% PCE remained (2000 h, air)	39
Buried interface	DL	$FA_{0.9}Cs_{0.1}PbI_3$	25.21	1.20	83.48	25.24	22.62	99.2% PCE remained (1200 h, air); 90% PCE remained (500 h, MPP)	118
Buried interface	KFSI	FAI/MAI/MACl	25.12	1.148	81.7	23.21	21.20	94% PCE remained (2264 h, 25 °C)	114
Buried interface	Rb^+	$FAPbI_3$	26.3	1.182	82.7	25.6	24.6	95% PCE remained (1000 h, shelf storage); 80% PCE remained (500 h, 85 °C, RH = 30-40%)	40
Buried interface	$FASnCI_x$	$FAPbI_3$	25.74	1.188	83.2	25.8	——	90% PCE remained (500 h)	41
Grain boundary	$(NpMA)_2PbI_4$	FAI/MAI/MACl	25.30	1.18	81.36	24.37	21.83	98% PCE remained (1500 h, MPP)	122
Grain boundary	DAB	$FA_{0.85}MA_{0.15}PbI_3$	25.21	1.19	82.61	24.83	22.37	95% PCE remained (1650 h, air); 89% PCE remained (500 h, 85 °C)	42
Grain boundary	PCA	$FAPbI_3$	24.9	1.195	84.3	25.1	23.6	90% PCE remained (2000 h, MPP)	129
Grain boundary	$(4AP)PbI_4$	$FAPbI_3$	25.7	1.18	81.81	24.9	22.7	97% PCE remained (1000 h, RH = 30%–40%)	130
Grain boundary	BA^+/PA^+	$FAPbI_3$	25.69	1.178	86.15	26.08	——	88% PCE remained (600 h, MPP)	110
Grain boundary	$HCOO^-$	$FAPbI_3$	26.35	1.189	81.7	25.59	23.86	85% PCE remained (400 h, MPP)	44
Grain boundary	OA^+, Cl^-	$MAPbI_3/FAPbI_3/Cs_xFA_{1-x}PbI_3$	25.3	1.17	84.2	24.95	21.99	81% PCE remained (1000 h, MPP)	131
Grain boundary	TOP	$FAPbI_3/MDACl_2/MACl$	26.1	1.17	81.7	24.9	24.4	—	45
Grain boundary	$CsPbBr_3$	$FAPbI_3$-$CsPbBr_3$	25.72	1.123	86.9	25.09	23.37	95% PCE remained (2100 h, air)	134
Grain boundary	TFAI	$FAPbI_3$	25.55	1.17	82.91	24.81	22.45	100% PCE remained (280 h, AM 1.5G)	135
Grain boundary	SPHI	RbCsFAMA-based PSCs	25.69	1.162	83.8	25.01	22.5	80% PCE remained (500 h, MPP)	143
Grain boundary	3AP	$FAPbI_3/MAPbI_3$	26.04	1.181	82.21	25.3	22.65	92% PCE remained (5000 h, air); 95% PCE remained (>500 h, MPP)	145
Top interface	$FcTc_2$	$Cs_{0.05}(FA_{0.98}MA_{0.02})_{0.95}Pb(I_{0.98}Br_{0.02})_3$	25.68	1.184	82.32	25.0	22.5	98% PCE remained (1500 h, AM 1.5G)	147
Top interface	3-APy	$(Rb_{0.05}Cs_{0.05}MA_{0.05}FA_{0.85})Pb(I_{0.95}Br_{0.05})_3$	26.09	1.16	83.82	25.37	22.85	87% PCE remained (2400 h, 1 sun, 65 °C, air)	112
Top interface	$DMePDAI_2$	$(FA_{0.85}MA_{0.1}Cs_{0.05})Pb(I_{2.9}Br_{0.1})$	25.25	1.158	84.3	24.7	20.9	90% PCE remained (1000 h, MPP)	149
Top interface	OLAI	$Cs_{0.03}(MA_{0.90}FA_{0.10})_{0.97}PbI_3$	24.69	1.2	82	24.3	22.3	95% PCE remained (500 h, MPP); 95% PCE remained (1200 h, 85 °C, RH = 85%)	31
Top interface	OA^+, TsO^-	$(FAPbI_3)_{0.95}(MAPbBr_3)_{0.05}$	25.32	1.166	82.65	24.41	21.7	100% PCE remained (800 h, MPP)	150
Multi-interface co-passivation	SID-PbI_2	$FAPbI_3/MAPbI_3$	25.36	1.152	83.80	24.47	22.60	82% PCE remained (7000 h, 20 °C, RH = 30%)	119
Multi-interface co-passivation	OA^+, GA^+, Cl^-	$(Cs_{0.05}FA_{0.75}MA_{0.20})Pb(I_{0.96}Br_{0.04})_3$	25.58	1.202	82.68	25.43	22.66	83% PCE remained (1200 h, MPP)	111
Multi-interface co-passivation	Cl^-	$FAPbI_3$	26.03	1.167	82.4	25.02	22.89	90% PCE remained (500 h, MPP)	43
Multi-interface co-passivation	Cl_2	FAI/MAI	25.40	1.168	81.58	24.21	22.76	80% PCE remained (905 h, MPP, 1 sun)	151

4. Outlook

Using two-dimensional (2D) perovskites has emerged as a highly effective strategy for enhancing the efficiency and stability of perovskite solar cells (PSCs). By passivating grain boundary defects, reducing ion migration channels and restricting ion migration, 2D/3D mixed perovskites have significantly improved device performance. However, several challenges remain that need to be addressed to fully leverage the benefits of 2D perovskite passivation.

Firstly, the concept of multi-interface cooperative passivation using 2D perovskites is not yet fully understood. Current strategies often focus on passivating a single interface, for instance, the buried interface, perovskite grain boundary interface or the top interface, while some studies have explored co-passivation approaches, where multiple interfaces were treated simultaneously. For instance, Chen *et al.*[108] used a guanidinium-based (GUA_2PbI_4) 2D perovskite to treat both the buried interface and the bulk of the PSCs, while Shen *et al.* employed a combination of octylammonium iodide (OAI) and guanidinium chloride (GACl) to modulate top interfaces, buried interfaces, and grain boundaries. And Ma *et al.* successfully post-treated the upper surface of a perovskite with a mixed solution of GUAI/tBPMAI, achieving an efficiency of 24.56%.[155] Despite these advances, there is a lack of comprehensive solutions that address all three interfaces effectively. The challenge lies in developing feasible buried interface passivation techniques that do not dissolve during subsequent processing steps, thereby enabling a truly multi-interface cooperative passivation strategy.

Secondly, the charge dynamics and transport mechanisms at a 2D/3D perovskite interface are not completely clear. The prevailing view is that 2D perovskite layers can improve the band structure and align energy levels, facilitating carrier extraction and transport while inhibiting recombination. However, recent studies have presented conflicting views. For instance, Yang *et al.* suggested that a 2D/3D interface operates as a type II heterojunction, promoting carrier extraction;[156] while Koch's team posited a type I heterojunction, which could inhibit carrier extraction.[157] Furthermore, some research indicates that 2D perovskites might impede carrier transport under illumination, contradicting the mainstream belief that they facilitate it.[158] These discrepancies highlight the need for further investigation into the charge dynamics and transport mechanisms at 2D/3D interfaces to provide a solid theoretical foundation for designing highly efficient and stable PSCs.

Thirdly, a deeper understanding of the degradation mechanism of 2D/3D PSCs is required. While 2D perovskites can improve the stability by providing hydrophobic long-chain cations and inhibiting ion migration, there are concerns about their long-term stability.[19,20,159] For instance, although 2D perovskite layers can improve moisture resistance and thermal stability, they may also increase ion migration, potentially compromising device stability. Studies have shown that 2D perovskites can cause negative work function migration, activating halide ion migration and thus reducing stability.[76,150,160] Moreover, Correa-Baena's group found that interface reconstruction involving a Ruddlesden–Popper structure can negatively affect thermal stability, suggesting that large cationic interface layers used in high-efficiency solar cells can induce instability.[161] Therefore, while 2D perovskite passivation offers significant benefits, its potential for achieving increased ion migration and other degradation pathways must be better understood mitigating the problems associated with it.

Addressing these challenges requires a multifaceted approach. Developing new methodologies for multi-interface cooperative passivation is crucial. This may involve innovative materials that can form stable, ultra-thin passivation layers resistant to dissolution during subsequent processing steps. Additionally, advanced characterization techniques should be employed to gain insights into the charge dynamics and transport mechanisms at 2D/3D interfaces. Computational modeling and experimental studies should go hand in hand to resolve the conflicting views and establish a clear understanding of how 2D perovskite layers interact with 3D perovskites. Furthermore, exploring the degradation mechanisms in detail will help identify and mitigate factors that limit the long-term stability of PSCs. This includes studying the interaction between different ions and perovskite materials, understanding the role of environmental factors such as humidity and temperature, and developing strategies to counteract negative effects like ion migration.

In summary, while 2D perovskite passivation has brought us closer to achieving highly efficient and stable PSCs, overcoming the current challenges requires concerted efforts in materials science, device engineering, and theoretical studies. By addressing these issues, we can unlock the full potential of 2D perovskite passivation paving the way for the commercial viability of PSCs.

Data availability

Data sharing is not applicable to this article as no new data were created or analyzed in this study.

Conflicts of interest

The authors declare no competing interests.

Acknowledgements

This work was financially supported by the Beijing Natural Science Foundation (No. 4222065 and JQ23020), and the National Natural Science Foundation of China (Grant No. 62034001, 52073005, 22033006).

References

1 W. Yin, T. Shi and Y. Yan, Unique Properties of Halide Perovskites as Possible Origins of the Superior Solar Cell Performance, *Adv. Mater.*, 2014, **26**, 4653–4658.

2 D. A. Egger, *et al.*, What Remains Unexplained about the Properties of Halide Perovskites?, *Adv. Mater.*, 2018, **30**, 1800691.
3 L. Fu, *et al.*, Defect passivation strategies in perovskites for an enhanced photovoltaic performance, *Energy Environ. Sci.*, 2020, **13**, 4017–4056.
4 A. K. Jena, A. Kulkarni and T. Miyasaka, Halide Perovskite Photovoltaics: Background, Status, and Future Prospects, *Chem. Rev.*, 2019, **119**, 3036–3103.
5 D. Luo, X. Li, A. Dumont, H. Yu and Z. Lu, Recent Progress on Perovskite Surfaces and Interfaces in Optoelectronic Devices, *Adv. Mater.*, 2021, **33**, 2006004.
6 J. Xue, R. Wang and Y. Yang, The surface of halide perovskites from nano to bulk, *Nat. Rev. Mater.*, 2020, **5**, 809–827.
7 A. Fakharuddin, *et al.*, Inorganic and Layered Perovskites for Optoelectronic Devices, *Adv. Mater.*, 2019, **31**, 1807095.
8 M. Lu, *et al.*, Metal Halide Perovskite Light-Emitting Devices: Promising Technology for Next-Generation Displays, *Adv. Funct. Mater.*, 2019, **29**, 1902008.
9 S. Liu, *et al.*, Buried interface molecular hybrid for inverted perovskite solar cells, *Nature*, 2024, **632**, 536–542.
10 H. Lin, *et al.*, Silicon heterojunction solar cells with up to 26.81% efficiency achieved by electrically optimized nanocrystalline-silicon hole contact layers, *Nat. Energy*, 2023, **8**, 789–799.
11 C. Ortiz-Cervantes, P. Carmona-Monroy and D. Solis-Ibarra, Two-Dimensional Halide Perovskites in Solar Cells: 2D or not 2D?, *ChemSusChem*, 2019, **12**, 1560–1575.
12 X. Zhang, *et al.*, Rapid degradation behavior of encapsulated perovskite solar cells under light, bias voltage or heat fields, *Nanoscale Adv.*, 2021, **3**, 6128–6137.
13 X. Zhang, *et al.*, Improved efficiency and stability of flexible perovskite solar cells by a new spacer cation additive, *RSC Adv.*, 2021, **11**, 33637–33645.
14 T. Zhou, Q. Li and L. Zhou, Fluorinated Quasi 2D Perovskite Solar Cells with Improved Stability and Over 19% Efficiency, *Adv. Energy Mater.*, 2024, 2400050.
15 P. Gao, A. R. Bin Mohd Yusoff and M. K. Nazeeruddin, Dimensionality engineering of hybrid halide perovskite light absorbers, *Nat. Commun.*, 2018, **9**, 5028.
16 G. Grancini and M. K. Nazeeruddin, Dimensional tailoring of hybrid perovskites for photovoltaics, *Nat. Rev. Mater.*, 2018, **4**, 4–22.
17 A. Krishna, S. Gottis, M. K. Nazeeruddin and F. Sauvage, Mixed Dimensional 2D/3D Hybrid Perovskite Absorbers: The Future of Perovskite Solar Cells?, *Adv. Funct. Mater.*, 2019, **29**, 1806482.
18 D. Sirbu, F. H. Balogun, R. L. Milot and P. Docampo, Layered Perovskites in Solar Cells: Structure, Optoelectronic Properties, and Device Design, *Adv. Energy Mater.*, 2021, **11**, 2003877.
19 X. Zhao, T. Liu and Y. Loo, Advancing 2D Perovskites for Efficient and Stable Solar Cells: Challenges and Opportunities, *Adv. Mater.*, 2022, **34**, 2105849.
20 J. Gong, M. Hao, Y. Zhang, M. Liu and Y. Zhou, Layered 2D Halide Perovskites beyond the Ruddlesden–Popper Phase: Tailored Interlayer Chemistries for High-Performance Solar Cells, *Angew. Chem.*, 2022, **134**, e202112022.
21 R. Azmi, *et al.*, Double-side 2D/3D heterojunctions for inverted perovskite solar cells, *Nature*, 2024, **628**, 93–98.
22 B. Febriansyah, *et al.*, Inorganic frameworks of low-dimensional perovskites dictate the performance and stability of mixed-dimensional perovskite solar cells, *Mater. Horiz.*, 2023, **10**, 536–546.
23 Q. Jiang, *et al.*, Surface passivation of perovskite film for efficient solar cells, *Nat. Photonics*, 2019, **13**, 460–466.
24 P. Zhao, B. J. Kim and H. S. Jung, Passivation in perovskite solar cells: A review, *Mater. Today Energy*, 2018, **7**, 267–286.
25 A. G. Aberle, Surface passivation of crystalline silicon solar cells: a review, *Prog. Photovolt. Res. Appl.*, 2000, **8**, 473–487.
26 E. H. Jung, *et al.*, Efficient, stable and scalable perovskite solar cells using poly(3-hexylthiophene), *Nature*, 2019, **567**, 511–515.
27 M. Chen, *et al.*, Enhanced efficiency and stability of perovskite solar cells by 2D perovskite vapor-assisted interface optimization, *J. Energy Chem.*, 2020, **45**, 103–109.
28 G. Yang, *et al.*, Stable and low-photovoltage-loss perovskite solar cells by multifunctional passivation, *Nat. Photonics*, 2021, **15**, 681–689.
29 A. H. Proppe, *et al.*, Multication perovskite 2D/3D interfaces form via progressive dimensional reduction, *Nat. Commun.*, 2021, **12**, 3472.
30 H. Chen, *et al.*, Quantum-size-tuned heterostructures enable efficient and stable inverted perovskite solar cells, *Nat. Photonics*, 2022, **16**, 352–358.
31 R. Azmi, *et al.*, Damp heat-stable perovskite solar cells with tailored-dimensionality 2D/3D heterojunctions, *Science*, 2022, **376**, 73–77.
32 R. Li, X. Liu and J. Chen, Opportunities and challenges of hole transport materials for high-performance inverted hybrid-perovskite solar cells, *Exploration*, 2023, **3**, 20220027.
33 L. Luo, *et al.*, Stabilization of 3D/2D perovskite heterostructures via inhibition of ion diffusion by cross-linked polymers for solar cells with improved performance, *Nat. Energy*, 2023, **8**, 294–303.
34 N. Li, *et al.*, Mixed Cation $FA_xPEA_{1-x}PbI_3$ with Enhanced Phase and Ambient Stability toward High-Performance Perovskite Solar Cells, *Adv. Energy Mater.*, 2017, **7**, 1601307.
35 A. A. Sutanto, *et al.*, In Situ Analysis Reveals the Role of 2D Perovskite in Preventing Thermal-Induced Degradation in 2D/3D Perovskite Interfaces, *Nano Lett.*, 2020, **20**, 3992–3998.
36 G. Grancini, *et al.*, One-Year stable perovskite solar cells by 2D/3D interface engineering, *Nat. Commun.*, 2017, **8**, 15684.
37 D. S. Lee, *et al.*, Passivation of Grain Boundaries by Phenethylammonium in Formamidinium-Methylammonium Lead Halide Perovskite Solar Cells, *ACS Energy Lett.*, 2018, **3**, 647–654.
38 C. Liang, *et al.*, Simultaneously boost diffusion length and stability of perovskite for high performance solar cells, *Nano Energy*, 2019, **59**, 721–729.
39 H. Huang, *et al.*, 24.8%-efficient planar perovskite solar cells via ligand-engineered TiO_2 deposition, *Joule*, 2022, **6**, 2186–2202.

40 Y. Zhao, *et al.*, Inactive $(PbI_2)_2RbCl$ stabilizes perovskite films for efficient solar cells, *Science*, 2022, **377**, 531–534.
41 H. Min, *et al.*, Perovskite solar cells with atomically coherent interlayers on SnO2 electrodes, *Nature*, 2021, **598**, 444–450.
42 W. Zhao, *et al.*, Orientation Engineering via 2D Seeding for Stable 24.83% Efficiency Perovskite Solar Cells, *Adv. Energy Mater.*, 2023, **13**, 2204260.
43 J. Wu, *et al.*, Regioselective Multisite Atomic-Chlorine Passivation Enables Efficient and Stable Perovskite Solar Cells, *J. Am. Chem. Soc.*, 2023, **145**, 5872–5879.
44 J. Jeong, *et al.*, Pseudo-halide anion engineering for α-$FAPbI_3$ perovskite solar cells, *Nature*, 2021, **592**, 381–385.
45 H. Min Relaxation of externally strained halide perovskite thin layers with neutral ligands.
46 M. Kim, *et al.*, Conformal quantum dot–SnO_2 layers as electron transporters for efficient perovskite solar cells, *Science*, 2022, **375**, 302–306.
47 Q. Jiang, *et al.*, Surface passivation of perovskite film for efficient solar cells, *Nat. Photonics*, 2019, **13**, 460–466.
48 H. Min, *et al.* Efficient, stable solar cells by using inherent bandgap of a-phase formamidinium lead iodide, (2019).
49 B. Park, *et al.*, Stabilization of formamidinium lead triiodide α-phase with isopropylammonium chloride for perovskite solar cells, *Nat. Energy*, 2021, **6**, 419–428.
50 F. Wang, *et al.*, Phenylalkylamine Passivation of Organolead Halide Perovskites Enabling High-Efficiency and Air-Stable Photovoltaic Cells, *Adv. Mater.*, 2016, **28**, 9986–9992.
51 X. Zhu, *et al.*, *In Situ* Grain Boundary Modification via Two-Dimensional Nanoplates to Remarkably Improve Stability and Efficiency of Perovskite Solar Cells, *ACS Appl. Mater. Interfaces*, 2018, **10**, 39802–39808.
52 Y. Wang, *et al.*, Efficient α-$CsPbI_3$ Photovoltaics with Surface Terminated Organic Cations, *Joule*, 2018, **2**, 2065–2075.
53 T. Wang, *et al.*, Phenethylammonium Functionalization Enhances Near-Surface Carrier Diffusion in Hybrid Perovskites, *J. Am. Chem. Soc.*, 2020, **142**, 16254–16264.
54 M. Degani, *et al.*, 23.7% Efficient inverted perovskite solar cells by dual interfacial modification, *Sci. Adv.*, 2021, **7**, eabj7930.
55 J. Zhuang, *et al.*, Interfacial Passivation for Perovskite Solar Cells: The Effects of the Functional Group in Phenethylammonium Iodide, *ACS Energy Lett.*, 2019, **4**, 2913–2921.
56 B. Yang, *et al.*, Interfacial Passivation Engineering of Perovskite Solar Cells with Fill Factor over 82% and Outstanding Operational Stability on n-i-p Architecture, *ACS Energy Lett.*, 2021, **6**, 3916–3923.
57 X. Feng, *et al.*, Perfection of Perovskite Grain Boundary Passivation by Eu-Porphyrin Complex for Overall-Stable Perovskite Solar Cells, *Adv. Sci.*, 2019, **6**, 1802040.
58 G. Kim, *et al.* Impact of strain relaxation on performance of a-formamidinium lead iodide perovskite solar cells. (2020).
59 Y. Liu, *et al.*, Ultrahydrophobic 3D/2D fluoroarene bilayer-based water-resistant perovskite solar cells with efficiencies exceeding 22%, *Sci. Adv.*, 2019, **5**, eaaw2543.
60 Y. Zhang, *et al.*, Bilateral Interface Engineering for Efficient and Stable Perovskite Solar Cells Using Phenylethylammonium Iodide, *ACS Appl. Mater. Interfaces*, 2020, **12**, 24827–24836.
61 Y. Zhu, *et al.*, Synergetic Passivation of Metal-Halide Perovskite with Fluorinated Phenmethylammonium toward Efficient Solar Cells and Modules, *Adv. Energy Mater.*, 2023, **13**, 2203681.
62 M. A. Mahmud, *et al.*, Double-Sided Surface Passivation of 3D Perovskite Film for High-Efficiency Mixed-Dimensional Perovskite Solar Cells, *Adv. Funct. Mater.*, 2020, **30**, 1907962.
63 M. Li, *et al.*, Brominated PEAI as Multi-Functional Passivator for High-Efficiency Perovskite Solar Cell, *Energy Environ. Mater.*, 2023, **6**, e12360.
64 Y. Li, *et al.*, Whether organic spacer cations induced 2D/3D or quasi-2D/3D mixed dimensional perovskites?, *Chem. Eng. J.*, 2022, **450**, 137887.
65 E. Jokar, *et al.*, Slow surface passivation and crystal relaxation with additives to improve device performance and durability for tin-based perovskite solar cells, *Energy Environ. Sci.*, 2018, **11**, 2353–2362.
66 Y. Zou, *et al.*, Highly efficient and stable 2D-3D perovskite solar cells fabricated by interfacial modification, *Nanotechnology*, 2019, **30**, 275202.
67 H. Lee, Y. Kang, S. Kwon, D. Kim and S. Na, Enhancing the Stability and Efficiency of Inverted Perovskite Solar Cells with a Mixed Ammonium Ligands Passivation Strategy, *Small Methods*, 2024, **8**, 2300948.
68 Y. Lv, *et al.*, Hexylammonium Iodide Derived Two-Dimensional Perovskite as Interfacial Passivation Layer in Efficient Two-Dimensional/Three-Dimensional Perovskite Solar Cells, *ACS Appl. Mater. Interfaces*, 2020, **12**, 698–705.
69 H. Zhang, *et al.*, Comparison of surface-passivation ability of the BAI salt and its induced 2D perovskite for high-performance inverted perovskite solar cells, *RSC Adv.*, 2021, **11**, 23249–23258.
70 X. Zhao, *et al.*, Effect of Steric Hindrance of Butylammonium Iodide as Interface Modification Materials on the Performance of Perovskite Solar Cells, *Sol. RRL*, 2022, **6**, 2200078.
71 J. Xu, *et al.*, Stable High-Efficiency $CsPbI_2Br$ Solar Cells by Designed Passivation Using Multifunctional 2D Perovskite, *Adv. Funct. Mater.*, 2022, **32**, 2202829.
72 H. Chen, *et al.*, Improved charge extraction in inverted perovskite solar cells with dual-site-binding ligands, *Science*, 2024, **384**, 189–193.
73 D. B. Khadka, Y. Shirai, M. Yanagida, T. Tadano and K. Miyano, Interfacial Embedding for High-Efficiency and Stable Methylammonium-Free Perovskite Solar Cells with Fluoroarene Hydrazine, *Adv. Energy Mater.*, 2022, **12**, 2202029.
74 Z. Li, *et al.*, Large-*n* quasi-phase-pure two-dimensional halide perovskite: A toolbox from materials to devices, *Sci. Bull.*, 2024, **69**, 382–418.

75 M. He, *et al.*, Compositional optimization of a 2D-3D heterojunction interface for 22.6% efficient and stable planar perovskite solar cells, *J. Mater. Chem. A*, 2020, **8**, 25831–25841.
76 S. Sidhik, *et al.*, Deterministic fabrication of 3D/2D perovskite bilayer stacks for durable and efficient solar cells, *Science*, 2022, **377**, 1425–1430.
77 Y. Bai, *et al.*, Dimensional Engineering of a Graded 3D-2D Halide Perovskite Interface Enables Ultrahigh V_{oc} Enhanced Stability in the p–i–n Photovoltaics, *Adv. Energy Mater.*, 2017, **7**, 1701038.
78 Y. Du, *et al.*, Manipulating the Formation of 2D/3D Heterostructure in Stable High-Performance Printable $CsPbI_3$ Perovskite Solar Cells, *Adv. Mater.*, 2023, **35**, 2206451.
79 Y. Zhong, *et al.*, Diammonium Molecular Configuration-Induced Regulation of Crystal Orientation and Carrier Dynamics for Highly Efficient and Stable 2D/3D Perovskite Solar Cells, *Angew. Chem., Int. Ed.*, 2022, **61**, e202114588.
80 Y. Choi, *et al.*, A vertically oriented two-dimensional Ruddlesden–Popper phase perovskite passivation layer for efficient and stable inverted perovskite solar cells, *Energy Environ. Sci.*, 2022, **15**, 3369–3378.
81 C. Luo, *et al.*, Facet orientation tailoring via 2D-seed-induced growth enables highly efficient and stable perovskite solar cells, *Joule*, 2022, **6**, 240–257.
82 S. Jeong, *et al.*, Cyclohexylammonium-Based 2D/3D Perovskite Heterojunction with Funnel-Like Energy Band Alignment for Efficient Solar Cells (23.91%), *Adv. Energy Mater.*, 2021, **11**, 2102236.
83 B. Han, *et al.*, Rational Design of Ferroelectric 2D Perovskite for Improving the Efficiency of Flexible Perovskite Solar Cells Over 23%, *Angew. Chem., Int. Ed.*, 2023, **62**, e202217526.
84 X. Yue, *et al.*, Surface Regulation through Dipolar Molecule Boosting the Efficiency of Mixed 2D/3D Perovskite Solar Cell to 24%, *Adv. Funct. Mater.*, 2023, **33**, 2209921.
85 Y. Yan, *et al.*, Polarity and moisture induced trans-grain-boundaries 2D/3D coupling structure for flexible perovskite solar cells with high mechanical reliability and efficiency, *Energy Environ. Sci.*, 2022, **15**, 5168–5180.
86 G. Li, *et al.*, Efficient and Stable 2D@3D/2D Perovskite Solar Cells Based on Dual Optimization of Grain Boundary and Interface, *ACS Energy Lett.*, 2021, **6**, 3614–3623.
87 G. Li, *et al.*, Surface defect passivation by 1,8-Naphthyridine for efficient and stable Formamidinium-based 2D/3D perovskite solar cells, *Chem. Eng. J.*, 2022, **449**, 137806.
88 S. Ahmad, *et al.*, Dion–Jacobson Phase 2D Layered Perovskites for Solar Cells with Ultrahigh Stability, *Joule*, 2019, **3**, 794–806.
89 P. Chen, *et al.*, In Situ Growth of 2D Perovskite Capping Layer for Stable and Efficient Perovskite Solar Cells, *Adv. Funct. Mater.*, 2018, **28**, 1706923.
90 J. Qiu, *et al.*, 2D Intermediate Suppression for Efficient Ruddlesden–Popper (RP) Phase Lead-Free Perovskite Solar Cells, *ACS Energy Lett.*, 2019, **4**, 1513–1520.
91 Y. Hu, *et al.*, Amino Acid-Based Low-Dimensional Management for Enhanced Perovskite Solar Cells, *Sol. RRL*, 2022, **6**, 2200168.
92 J.-H. Kim, S.-G. Kim and N.-G. Park, Effect of Chemical Bonding Nature of Post-Treatment Materials on Photovoltaic Performance of Perovskite Solar Cells, *ACS Energy Lett.*, 2021, **6**, 3435–3442.
93 N. Wei, *et al.*, Post-Treatment-Free Dual-Interface Passivation via Facile 1D/3D Perovskite Heterojunction Construction, *JACS Au*, 2023, **3**, 3324–3332.
94 N. Yang, *et al.*, An *in situ* cross-linked 1D/3D perovskite heterostructure improves the stability of hybrid perovskite solar cells for over 3000 h operation, *Energy Environ. Sci.*, 2020, **13**, 4344–4352.
95 T. Wang, *et al.*, Dimensional Regulation from 1D/3D to 2D/3D of Perovskite Interfaces for Stable Inverted Perovskite Solar Cells, *J. Am. Chem. Soc.*, 2024, **146**, 7555–7564.
96 C. Zuo, *et al.*, Self-Assembled 2D Perovskite Layers for Efficient Printable Solar Cells, *Adv. Energy Mater.*, 2019, **9**, 1803258.
97 X. Chen, *et al.*, Self-Assembly of 2D/3D Perovskites by Crystal Engineering for Efficient Air-Processed, Air-Stable Inverted Planar Perovskite Solar Cells, *ACS Appl. Energy Mater.*, 2020, **3**, 2975–2982.
98 S. Wang, *et al.*, Two birds with one stone: Simultaneous realization of constructed 3D/2D heterojunction and p-doping of hole transport layer for highly efficient and stable perovskite solar cells, *Chem. Eng. J.*, 2023, **453**, 139721.
99 J. Wang, *et al.*, Bottom-Up Templated and Oriented Crystallization for Inverted Triple-Cation Perovskite Solar Cells with Stabilized Nickel-Oxide Interface, *Small*, 2022, **18**, 2203886.
100 S. Wang, *et al.*, Ion-Dipole Interaction for Self-Assembled Monolayers: A New Strategy for Buried Interface in Inverted Perovskite Solar Cells, *Adv. Funct. Mater.*, 2024, 2316202.
101 H. Tang, *et al.*, Reinforcing self-assembly of hole transport molecules for stable inverted perovskite solar cells, *Science*, 2024, **383**, 1236–1240.
102 J. Xu, *et al.*, Anion optimization for bifunctional surface passivation in perovskite solar cells, *Nat. Mater.*, 2023, **22**, 1507–1514.
103 D. Yu, *et al.*, Electron-withdrawing organic ligand for high-efficiency all-perovskite tandem solar cells, *Nat. Energy*, 2024, **9**, 298–307.
104 E. Aydin, *et al.*, Enhanced optoelectronic coupling for perovskite/silicon tandem solar cells, *Nature*, 2023, **623**, 732–738.
105 D. Xu, P. Wu and H. Tan, Self-assembled monolayers for perovskite solar cells, *Inf. Funct. Mater.*, 2024, **1**, 2–25.
106 J. Zeng, L. Bi, Y. Cheng, B. Xu and A. K.-Y. Jen, Self-assembled monolayer enabling improved buried interfaces in blade-coated perovskite solar cells for high efficiency and stability, *Nano Res. Energy*, 2022, **1**, e9120004.
107 X. Zhang, *et al.*, Dual Optimization of Bulk and Surface via Guanidine Halide for Efficient and Stable 2D/3D Hybrid

Perovskite Solar Cells, *Adv. Energy Mater.*, 2022, **12**, 2201105.
108 B. Chen, *et al.*, Passivation of the Buried Interface via Preferential Crystallization of 2D Perovskite on Metal Oxide Transport Layers, *Adv. Mater.*, 2021, **33**, 2103394.
109 Y. Zhang, *et al.*, Depth-dependent defect manipulation in perovskites for high-performance solar cells, *Energy Environ. Sci.*, 2021, **14**, 6526–6535.
110 J. Park, *et al.*, Controlled growth of perovskite layers with volatile alkylammonium chlorides, *Nature*, 2023, **616**, 724–730.
111 L. Shen, *et al.*, Ion-Diffusion Management Enables All-Interface Defect Passivation of Perovskite Solar Cells, *Adv. Mater.*, 2023, **35**, 2301624.
112 Q. Jiang, *et al.*, Surface reaction for efficient and stable inverted perovskite solar cells, *Nature*, 2022, **611**, 278–283.
113 Z. Ni, *et al.*, Resolving spatial and energetic distributions of trap states in metal halide perovskite solar cells, *Science*, 2020, **367**, 1352–1358.
114 C. Gong, *et al.*, Stabilizing Buried Interface via Synergistic Effect of Fluorine and Sulfonyl Functional Groups Toward Efficient and Stable Perovskite Solar Cells, *Nano-Micro Lett.*, 2023, **15**, 17.
115 X. Zuo, *et al.*, Passivating buried interface via self-assembled novel sulfonium salt toward stable and efficient perovskite solar cells, *Chem. Eng. J.*, 2022, **431**, 133209.
116 B. Chen, P. N. Rudd, S. Yang, Y. Yuan and J. Huang, Imperfections and their passivation in halide perovskite solar cells, *Chem. Soc. Rev.*, 2019, **48**, 3842–3867.
117 Z. Gao, Y. Wang and W. C. H. Choy, Buried Interface Modification in Perovskite Solar Cells: A Materials Perspective, *Adv. Energy Mater.*, 2022, **12**, 2104030.
118 L. Yang, *et al.*, 25.24%-Efficiency $FACsPbI_3$ Perovskite Solar Cells Enabled by Intermolecular Esterification Reaction of DL-Carnitine Hydrochloride, *Adv. Mater.*, 2023, **35**, 2211545.
119 T. Li, *et al.*, Auxiliary Buried-Interface Passivation Toward Stable and Low-Recombination-Loss Perovskite Photovoltaics, *Small Sci.*, 2024, **4**, 2300218.
120 Q. Jiang, *et al.*, Planar-Structure Perovskite Solar Cells with Efficiency beyond 21%, *Adv. Mater.*, 2017, **29**, 1703852.
121 Y. Chen, *et al.*, Mechanism of PbI_2 in Situ Passivated Perovskite Films for Enhancing the Performance of Perovskite Solar Cells, *ACS Appl. Mater. Interfaces*, 2019, **11**, 44101–44108.
122 T. Zhou, *et al.*, Crystal Growth Regulation of 2D/3D Perovskite Films for Solar Cells with Both High Efficiency and Stability, *Adv. Mater.*, 2022, **34**, 2200705.
123 L. N. Quan, *et al.*, Ligand-Stabilized Reduced-Dimensionality Perovskites, *J. Am. Chem. Soc.*, 2016, **138**, 2649–2655.
124 L. Yan, *et al.*, Charge-Carrier Transport in Quasi-2D Ruddlesden–Popper Perovskite Solar Cells, *Adv. Mater.*, 2022, **34**, 2106822.
125 L. Zhao, *et al.*, Enabling full-scale grain boundary mitigation in polycrystalline perovskite solids, *Sci. Adv.*, 2022, **8**, eabo3733.
126 J. Cheng, *et al.*, A Universal Microscopic Patterned Doping Method for Perovskite Enables Ultrafast, Self-Powered, Ultrasmall Perovskite Photodiodes, *Adv. Mater.*, 2023, **35**, 2300691.
127 J. Cao, *et al.*, Enhanced Performance of Planar Perovskite Solar Cells Induced by van der Waals Epitaxial Growth of Mixed Perovskite Films on WS_2 Flakes, *Adv. Funct. Mater.*, 2020, **30**, 2002358.
128 H. Zhang, *et al.*, Bottom-Up Quasi-Epitaxial Growth of Hybrid Perovskite from Solution Process-Achieving High-Efficiency Solar Cells via Template-Guided Crystallization, *Adv. Mater.*, 2021, **33**, 2100009.
129 Z. Shen, *et al.*, Crystal-array-assisted growth of a perovskite absorption layer for efficient and stable solar cells, *Energy Environ. Sci.*, 2022, **15**, 1078–1085.
130 T. Yang, *et al.*, Amidino-based Dion–Jacobson 2D perovskite for efficient and stable 2D/3D heterostructure perovskite solar cells, *Joule*, 2023, **7**, 574–586.
131 H. Wang, *et al.*, Pre-annealing treatment for high-efficiency perovskite solar cells via sequential deposition, *Joule*, 2022, **6**, 2869–2884.
132 X. Zhang, *et al.*, Phase Transition Control for High Performance Ruddlesden–Popper Perovskite Solar Cells, *Adv. Mater.*, 2018, **30**, 1707166.
133 J. M. Hoffman, *et al.*, In Situ Grazing-Incidence Wide-Angle Scattering Reveals Mechanisms for Phase Distribution and Disorientation in 2D Halide Perovskite Films, *Adv. Mater.*, 2020, **32**, 2002812.
134 X. Li, *et al.*, Modulating the deep-level defects and charge extraction for efficient perovskite solar cells with high fill factor over 86%, *Energy Environ. Sci.*, 2022, **15**, 4813–4822.
135 Z. Shi, *et al.*, Room Temperature Crystallized Phase-Pure α-$FAPbI_3$ Perovskite with In-Situ Grain-Boundary Passivation, *Adv. Sci.*, 2024, 2400275.
136 N. Wu, *et al.*, Stabilizing Precursor Solution and Controlling Crystallization Kinetics Simultaneously for High-Performance Perovskite Solar Cells, *Adv. Mater.*, 2023, **35**, 2304809.
137 D. Bi, *et al.*, Efficient luminescent solar cells based on tailored mixed-cation perovskites, *Sci. Adv.*, 2016, **2**, e1501170.
138 T. J. Jacobsson, *et al.*, Unreacted PbI_2 as a Double-Edged Sword for Enhancing the Performance of Perovskite Solar Cells, *J. Am. Chem. Soc.*, 2016, **138**, 10331–10343.
139 J. Yang, *et al.*, Precise control of PbI_2 excess into grain boundary for efficacious charge extraction in off-stoichiometric perovskite solar cells, *Electrochim. Acta*, 2020, **338**, 135697.
140 Y. Chen, *et al.*, In Situ Management of Ions Migration to Control Hysteresis Effect for Planar Heterojunction Perovskite Solar Cells, *Adv. Funct. Mater.*, 2022, **32**, 2108417.
141 Y. Sui, *et al.*, Understanding the Role of Crown Ether Functionalization in Inverted Perovskite Solar Cells, *ACS Energy Lett.*, 2024, **9**, 1518–1526.
142 L. Xie, *et al.*, A Deformable Additive on Defects Passivation and Phase Segregation Inhibition Enables the Efficiency of

Inverted Perovskite Solar Cells over 24%, *Adv. Mater.*, 2023, **35**, 2302752.
143 Q. Wang, *et al.*, Over 25% efficiency and stable bromine-free RbCsFAMA-based quadruple cation perovskite solar cells enabled by an aromatic zwitterion, *J. Mater. Chem. A*, 2023, **11**, 1170–1179.
144 W. Zhou, *et al.*, The Role of Grain Boundaries on Ion Migration and Charge Recombination in Halide Perovskites, *Small*, 2024, 2310368.
145 T. Yang, *et al.*, One-stone-for-two-birds strategy to attain beyond 25% perovskite solar cells, *Nat. Commun.*, 2023, **14**, 839.
146 J. J. Yoo, *et al.*, An interface stabilized perovskite solar cell with high stabilized efficiency and low voltage loss, *Energy Environ. Sci.*, 2019, **12**, 2192–2199.
147 Z. Li, *et al.*, Organometallic-functionalized interfaces for highly efficient inverted perovskite solar cells, *Science*, 2022, **376**, 416–420.
148 T. Bu, *et al.*, Structure engineering of hierarchical layered perovskite interface for efficient and stable wide bandgap photovoltaics, *Nano Energy*, 2020, **75**, 104917.
149 F. Zhang, *et al.*, Metastable Dion-Jacobson 2D structure enables efficient and stable perovskite solar cells, *Science*, 2022, **375**, 71–76.
150 S. Tan, *et al.*, Stability-limiting heterointerfaces of perovskite photovoltaics, *Nature*, 2022, **605**, 268–273.
151 Y. Luo, *et al.*, Dissolved-Cl_2 triggered redox reaction enables high-performance perovskite solar cells, *Nat. Commun.*, 2023, **14**, 3738.
152 F. Wang, *et al.*, Modulating Crystallization and Defect Passivation by Butyrolactone Molecule for Perovskite Solar Cells, *Molecules*, 2023, **28**, 5542.
153 M. Wang, *et al.*, Synergetic Co-Modulation of Crystallization and Co-Passivation of Defects for $FAPbI_3$ Perovskite Solar Cells, *Adv. Funct. Mater.*, 2022, **32**, 2108567.
154 S. Gharibzadeh, *et al.*, Two birds with one stone: dual grain-boundary and interface passivation enables >22% efficient inverted methylammonium-free perovskite solar cells, *Energy Environ. Sci.*, 2021, **14**, 5875–5893.
155 H. Ma, *et al.*, Asymmetric organic diammonium salt buried in SnO_2 layer enables fast carrier transfer and interfacial defects passivation for efficient perovskite solar cells, *Chem. Eng. J.*, 2022, **442**, 136291.
156 J. Yang, *et al.*, Energetics and Energy Loss in 2D Ruddlesden–Popper Perovskite Solar Cells, *Adv. Energy Mater.*, 2020, **10**, 2000687.
157 D. Shin, *et al.*, The Electronic Properties of a 2D Ruddlesden–Popper Perovskite and its Energy Level Alignment with a 3D Perovskite Enable Interfacial Energy Transfer, *Adv. Funct. Mater.*, 2023, **33**, 2208980.
158 D. Yu, *et al.*, Direct observation of photoinduced carrier blocking in mixed-dimensional 2D/3D perovskites and the origin, *Nat. Commun.*, 2022, **13**, 6229.
159 T. Zhang, C. Hu and S. Yang, Ion Migration: A ''Double-Edged Sword'' for Halide-Perovskite-Based Electronic Devices, *Small Methods*, 2020, **4**, 1900552.
160 J. Chen, J. Seo and N. Park, Simultaneous Improvement of Photovoltaic Performance and Stability by In Situ Formation of 2D Perovskite at $(FAPbI_3)_{0.88}(CsPbBr_3)_{0.12}$/CuSCN Interface, *Adv. Energy Mater.*, 2018, **8**, 1702714.
161 C. A. R. Perini, *et al.*, Interface Reconstruction from Ruddlesden–Popper Structures Impacts Stability in Lead Halide Perovskite Solar Cells, *Adv. Mater.*, 2022, **34**, 2204726.